研究成果の刊行物・別刷

THE JOURNAL OF BIOLOGICAL CHEMISTRY VOL. 280, NO. 52, pp. 42759–42765, December 30, 2005

Cholesterol-mediated Neurite Outgrowth Is Differently Regulated between Cortical and Hippocampal Neurons*[S]

Received for publication, August 19, 2005, and in revised form, October 24, 2005 Published, JBC Papers in Press, November 2, 2005, DOI 10.1074/jbc.M509164200

Mihee Ko, Kun Zou, Hirohisa Minagawa, Wenxin Yu, Jian-Sheng Gong, Katsuhiko Yanagisawa, and Makoto Michikawa[1]

From the Department of Alzheimer's Disease Research, National Institute for Longevity Sciences, 36-3 Gengo, Morioka, Obu, Aichi 474-8522, Japan

The acquisition of neuronal type-specific morphogenesis is a central feature of neuronal differentiation and has important consequences for region-specific nervous system functions. Here, we report that the cell type-specific cholesterol profile determines the differential modulation of axon and dendrite outgrowths in hippocampal and cerebral cortical neurons in culture. The extent of axon and dendrite outgrowths is greater and the polarity formation occurs earlier in cortical neurons than in hippocampal neurons. The cholesterol concentrations in total homogenate and the lipid rafts from hippocampal neurons are significantly higher than those from cortical neurons. Cholesterol depletion by β-cyclodextrin markedly enhanced the neurite outgrowth and accelerated the establishment of neuronal polarity in hippocampal neurons, which were similarly observed in nontreated cortical neurons, whereas cholesterol loading had no effects. In contrast, both depletion and loading of cholesterol decreased the neurite outgrowths in cortical neurons. The stimulation of neurite outgrowth and polarity formation induced by cholesterol depletion was accompanied by an enhanced localization of Fyn, a Src kinase, in the lipid rafts of hippocampal neurons. A concomitant treatment with β-cyclodextrin and a Src family kinase inhibitor, PP2, specifically blocked axon outgrowth but not dendrite outgrowth (both of which were enhanced by β-cyclodextrin) in hippocampal neurons, suggesting that axon outgrowth modulated by cholesterol is induced in a Fyn-dependent manner. These results suggest that cellular cholesterol modulates axon and dendrite outgrowths and neuronal polarization under culture conditions and also that the difference in cholesterol profile between hippocampal and cortical neurons underlies the difference in neurite outgrowth between these two types of neurons.

Neurons contain two types of processes, axons and dendrites, which are structurally and functionally distinct and play different roles in the maintenance of brain functions. There are studies showing the significant role of lipids in the formation of neuronal polarity; it has been shown that phospholipids regulate neurite outgrowth in cultured neurons (1) and that the correct distribution of axonal membrane proteins requires the formation of sphingomyelin/cholesterol-rich microdomains, lipid rafts, and the maturation of the axonal plasma membrane requires the up-regulation of sphingomyelin synthesis (2, 3). Cholesterol also plays a prominent role in raft-mediated trafficking and sorting, because cholesterol depletion by methyl-β-cyclodextrin impedes trafficking from the trans-Golgi network to the apical membrane (4). It has been shown that cholesterol modulates dendrite outgrowth (5), that its deficiency enhances phosphorylation of tau and axonal depolymerization (6), and that axonal regeneration is dependent on local cholesterol reutilization *in vivo* (7). In addition, cholesterol supplied as glial lipoproteins stimulates the axon outgrowth of central nervous system neurons (8, 9). Moreover, previous studies have shown that glia-derived cholesterol is essential for synaptogenesis and synaptic plasticity (10, 11). These lines of evidence suggest that membrane lipids play essential roles in neurite outgrowth and the formation of synapse neuronal polarity.

The region-specific difference in the development of Alzheimer disease pathologies is known. For example, the initial amyloid-β protein deposition occurs in poorly myelinated areas of the basal neocortex and spreads into adjoining areas and the hippocampus, whereas the formation of neurofibrillary tangles, which contain hyperphosphorylated tau, preferentially occurs in the transentorhinal region and hippocampus in the absence of amyloid deposits (12–14). Previous studies have suggested that the altered cholesterol metabolism is associated with the development of Alzheimer disease (for review, see Ref. 15) via the modulation of amyloid-β synthesis (16, 17). Other lines of evidence suggest that cholesterol plays essential roles in the modulation of tau phosphorylation (6, 18, 19), neurofibrillary tangle formation (20), and neuronal survival (21, 22). These lines of evidence suggest that Alzheimer disease pathologies preferentially developing in specific brain regions may be explained by a region-specific difference in the lipid profile. However, the region-specific profiles of lipids in neurons and their effects on neuronal functions remain to be clarified. The present study was designed to determine whether there is any difference in the profiles of lipids in primary cultured neurons isolated from different regions, namely, the mouse cerebral cortices and hippocampus, and whether neuronal function, including neurite outgrowth and polarity formation, is modulated by cellular lipids.

MATERIALS AND METHODS

Cell Culture—Neuron-rich cultures were prepared from the cerebral cortices and hippocampi of rat brains on embryonic day 18. The isolated cerebral cortices and hippocampi were incubated in 2 ml of Hepes-buffered saline solution containing 0.25% trypsin-EDTA for 20 min at 37 °C. The tissues were then washed three times in Dulbecco's modified Eagle's medium (DMEM)[2] containing 10% fetal bovine serum. The tissues in 1 ml of DMEM containing 10% fetal bovine serum were sub-

* This work was supported by Grants H14-10 (Comprehensive Research on Aging and Health) and H17-004 (Research on Human Genome and Tissue Engineering) from the Ministry of Health, Labor, and Welfare of Japan and by the Program for Promotion of Fundamental Studies in Health of the National Institute of Biomedical Innovation, Japan. The costs of publication of this article were defrayed in part by the payment of page charges. This article must therefore be hereby marked "*advertisement*" in accordance with 18 U.S.C. Section 1734 solely to indicate this fact.

[S] The on-line version of this article (available at http://www.jbc.org) contains supplemental Figs. S1 and S2 and Experimental Procedures.

[1] To whom correspondence should be addressed. Tel.: 81-562-46-2311; Fax: 81-562-46-8569; E-mail: michi@nils.go.jp.

[2] The abbreviations used are: DMEM, Dulbecco's modified Eagle's medium; PBS, phosphate-buffered saline; β-CD, methyl-β-cyclodextrin; Mes, 4-morpholineethanesulfonic acid.

jected to gentle pipetting using a micropipette (Gilson) 10 times and to further pipetting using a fire-polished glass Pasteur pipette 10 times. The volume of solution containing dissociated tissues was adjusted to 10 ml by adding DMEM containing 10% fetal bovine serum, and the tissues were obtained as pellets by centrifugation at 800 rpm for 5 min. The samples were washed two times in DMEM by centrifugation at 800 rpm for 5 min. The dissociated cells were suspended in feeding medium (consisting of DMEM/F12 (50:50%) nutrient mixture and N_2 supplements) and plated onto poly-D-lysine-coated 12-well plates at a cell density of $5 \times 10^3/cm^2$. More than 99% of the cultured cells were identified as neurons by immunocytochemical analysis using a monoclonal antibody against microtubule-associated protein 2, a neuron-specific marker, on day 3 of culture (21).

Morphological Analysis—The cultured neurons were washed three times in PBS and incubated in PBS containing 4% paraformaldehyde for 15 min at room temperature. The cells were then washed three times in PBS and incubated in PBS containing 0.2% Triton X-100 and 1% bovine serum albumin for 15 min at room temperature. The cells were washed three times in PBS and incubated with a monoclonal anti-β-tubulin antibody (Covance, Berkeley, CA) at 2 μg/ml overnight at 4 °C. The cultured cells were then washed in PBS three times, and the anti-β-tubulin antibody bound to neuronal β-tubulin was visualized using an ABC kit (Vector Laboratories, Burlingame, CA). The photographs of stained neurons were captured using a charge-coupled device camera (DC500) (Leica Microsystems GMBH, Wetzar, Germany) attached to a phase-contrast microscope (Olympus IX70, Olympus Co., Ltd., Tokyo, Japan). The length of axons and dendrites/cell and the ratio of neurite number/cell were determined using an image analyzer (KS400, Karl Zeiss Co., Ltd., Jena, Germany). Longest-axon length, axonal plexus length, and total dendrite length are defined in supplemental Fig. S1.

Lipid Analysis—For the extraction of cellular lipids, dried cells were incubated in hexane:isopropanol (3:2 v/v) for 1 h at room temperature. The solvent in each plate was collected and dried under N_2 gas. The organic phases were redissolved in 400 μl of chloroform, and a 150-μl sample was transferred onto 96-well polypropylene plates (Corning Coster, Corning, NY) and dried under air flow. The dried lipids were then dissolved in 20 μl of isopropanol. The concentration of cholesterol was determined using a cholesterol determination kit, LTCII (Kyowa Medex, Tokyo), and the concentration of phospholipids was determined using a phospholipid determination kit, PLB (Wako, Osaka, Japan) as described previously (23).

Immunoblot Analysis—Immunoblot analysis was performed as described previously (18). The primary antibodies used were mouse monoclonal antibodies, Fyn sc-434 (1: 1,000 dilution, Santa Cruz Biotechnology, Inc.), flotillin (1:1000 dilution, BD Biosciences), and NCAM (1:1000 dilution, Chemicon International, Inc.). GM1 was detected using cholera toxin B-conjugated horseradish peroxidase (1:10,000, Sigma-Aldrich). After rinsing and incubation in the presence of an appropriate peroxidase-conjugated secondary antibody, the bands were detected with an ECL kit (Amersham Biosciences). Protein concentrations were determined using the bicinchoninic acid protein assay kit (Pierce).

Cholesterol Depletion and Drug Treatment—A stock solution of methyl-β-cyclodextrin (β-CD) (Sigma-Aldrich) was prepared by dissolving β-CD in DMEM/F12 medium at a concentration of 100 mM. For cholesterol depletion, neurons were treated with β-CD at a final concentration of 5 mM for 10 min at 37 °C, washed in the culture medium three times, and then cultured further for 5, 24, or 48 h. Cholesterol (Sigma-Aldrich) and PP2 (Calbiochem) were dissolved in 100% ethanol to prepare stock solutions at concentrations of 7 mg/ml and 5 mM, respectively. Cholesterol and PP2 solutions were diluted and used at final concentrations of 7 μg/ml and 5 μM, respectively.

Lipid Raft Fractions—Sucrose gradients were prepared by established methods with modifications (24, 25). Neurons were rinsed with PBS and scraped and homogenized with 1 ml of Mes-buffered saline (25 mM Mes, pH 6.5, 0.15 M NaCl) containing 1% Triton X-100, a mixture of protease inhibitors, Complete™, and phosphatase inhibitors. Extracts containing 350 μg of proteins were subjected to sucrose gradient analysis. Gradients were centrifuged for 20 h at 44,800 rpm at 4 °C in a SW 50.1 rotor (Beckman Instruments). Fractions (400 μl) were collected sequentially starting from the top of the gradient. The extraction of lipids and the subsequent determination of the concentrations of cholesterol and phospholipid in each sample were carried out according to previously described methods (23).

Triton X-100-soluble and -insoluble Fractions—Cultured neurons (1×10^6 cells) were washed three times with ice-cold PBS and scraped in 200 μl of 1% Triton X-100 in Mes-buffered saline. Neurons were lysed by pipetting 10 times followed by ultrasonication for 5 min at a high level at 4 °C in a Bioruptor (Cosmo Bio, Tokyo). Triton X-100-soluble and -insoluble fractions were separated by centrifugation at 100,000 × *g* for 60 min using a TLA-100 rotor (Beckman Instruments). The resulting pellet (Triton X-100-insoluble fraction) was washed with PBS three times and resuspended in 100 μl of radioimmune precipitation assay buffer; the resultant supernatant was used in lipid analysis. The supernatant, *i.e.* the Triton X-100-soluble fraction, was used in lipid analysis.

Statistical Analyses—All statistical analyses were conducted using the StatView 5.0 software package (Abacus Concepts Inc., Berkeley, CA). The data are expressed as means ± S.E., and statistical significance was assessed by an analysis of variance followed by post-hoc Fisher's PLSD test. A value of $p < 0.05$ was considered statistically significant.

RESULTS

Differential Neurite Outgrowth in Cultured Neurons Prepared from the Hippocampi and Cortices of Rat Embryos—Primary neurons were prepared from the hippocampi and cortices of rat embryos on embryonic day 18 and maintained for 1, 3, and 5 days in serum-free N_2-supplemented culture medium. The cultures were then stained with the anti-β-tubulin antibody. Cortical neurons immunostained with the anti-tubulin antibody on culture days 1, 3, and 5 are shown in Fig. 1, *a*, *c*, and *e*, respectively. Hippocampal neurons immunostained with the same antibody on culture days 1, 3, and 5 are shown in Fig. 1, *b*, *d*, and *f*, respectively. Cortical neurons had longer axons and dendrites than hippocampal neurons at each time point examined. The longest-axon length, axonal plexus length, dendrite length, and number of neurites were determined as described under "Materials and Methods" (see also supplemental Fig. S1). The longest-axon length and total dendrite length were greater in cortical neurons than in hippocampal neurons; these lengths increased with culture time in both types of neurons (Fig. 1, *g* and *i*). The axonal plexus length of cortical neurons on culture day 5 was greater than that of hippocampal neurons (Fig. 1*h*). In contrast, the number of neurites per cortical neuron on culture day 5 was similar to the number of neurites per hippocampal neuron (Fig. 1*j*).

Differential Lipid Profiles in Cultured Neurons Prepared from the Hippocampi and Cortices of Rat Embryos—We next determined the concentrations of cholesterol and phospholipids in these neurons. The cholesterol concentration in hippocampal neurons was significantly higher than in cortical neurons (Fig. 2*a*); however, the concentration of phospholipids was similar between these two types of neurons (Fig. 2*b*). The concentrations of cholesterol and phospholipids in Triton X-100-soluble and -insoluble fractions in each neuronal culture were also

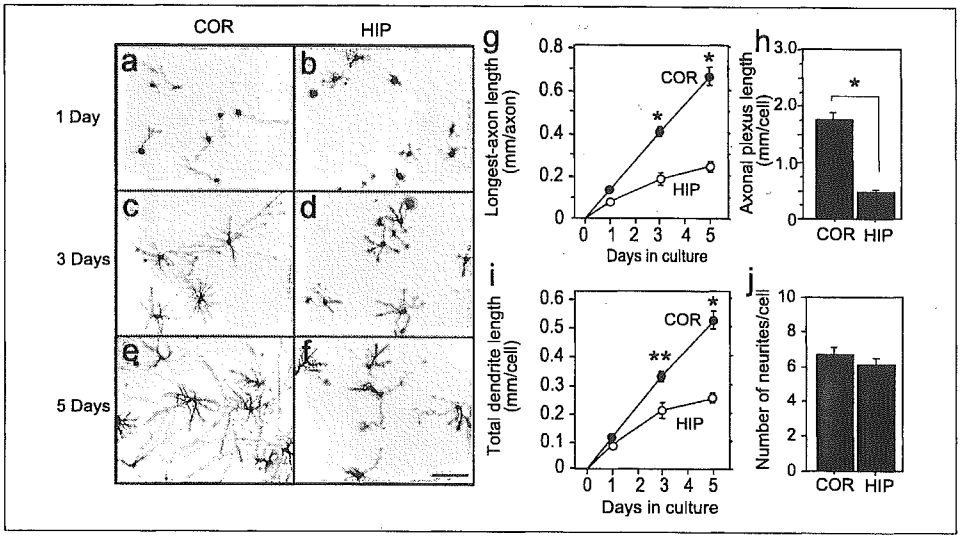

FIGURE 1. **Difference in neurite outgrowth between cortical and hippocampal neurons in culture.** Primary neurons were prepared from cortices and hippocampi of rat brains on embryonic day 18 and plated on poly-D-lysine-coated 12-well plastic plates at a cell density of 5×10^3/well. *a–f*, the neurons were cultured in serum-free N_2-supplemented medium (N_2-medium) and fixed and immunostained with anti-β-tubulin antibody on the days indicated. *Scale bar* represents 100 μm. *COR* and *HIP* represent cortical neurons and hippocampal neurons, respectively. Neurons from stages 3–5 (26) were analyzed. Longest-axon length (*g*) and total dendrite length (*i*) per neuron on days 1, 3, and 5 in culture were determined. Axonal plexus length (*h*) and number of neurites (*j*) per neuron were determined on culture day 5. The number of neurons analyzed was 25 in each culture. *, $p < 0.0001$, and **, $p < 0.005$, between cortical and hippocampal neurons. Four independent experiments showed similar results.

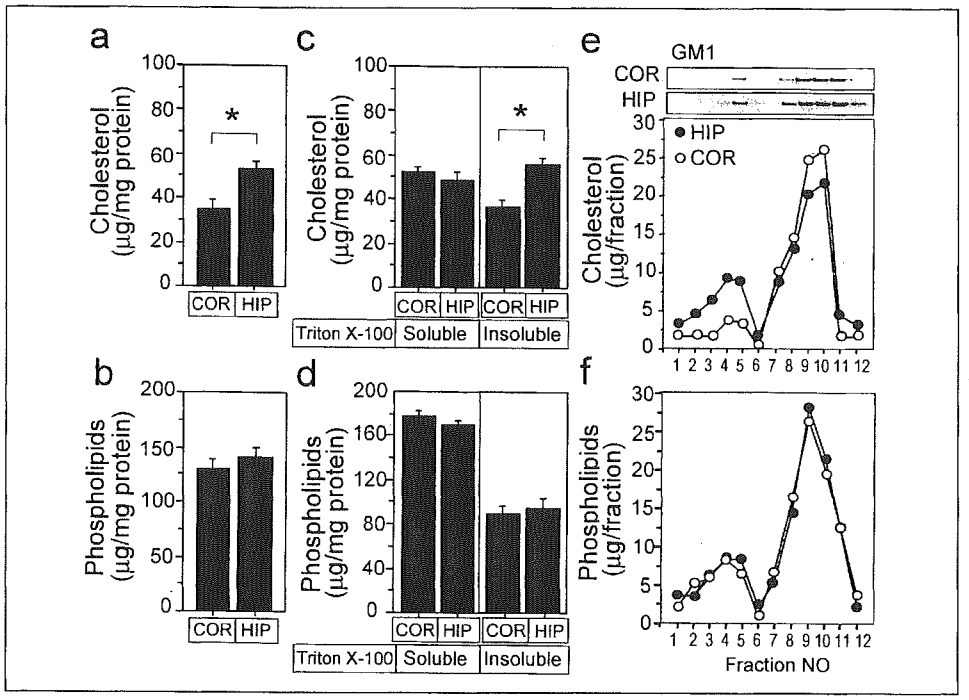

FIGURE 2. **Characterization of lipid profiles of cortical and hippocampal neurons.** Cholesterol and phospholipid concentrations in cortical and hippocampal neurons cultured in N_2-medium for 5 days were analyzed as described under "Materials and Methods." The concentrations of cholesterol (*a*) and phospholipids (*b*) in hippocampal (*HIP*) and cortical (*COR*) neurons per mg of protein were determined. In addition, the concentrations of cholesterol (*c*) and phospholipids (*d*) in the Triton X-100-soluble and -insoluble fraction from hippocampal and cortical neurons were determined. The data represent mean ± S.E. The number of samples was six for each treatment. *, $p < 0.05$. Three independent experiments showed similar results. Isolation of lipid raft fractions from cultured hippocampal and cortical neurons was performed by sucrose density gradient ultracentrifugation, and cholesterol (*e*) and phospholipid (*f*) levels in each fraction are shown.

determined. The cholesterol concentration in the Triton X-100-insoluble fraction from hippocampal neurons was higher than that from cortical neurons, whereas the concentration in the Triton X-100-soluble fraction from hippocampal neurons was similar to that from cortical neurons (Fig. 2*c*). There were no significant differences in the concentrations of phospholipids in the Triton X-100-soluble and -insoluble fractions between hippocampal and cortical neurons (Fig. 2*d*). Because cholesterol concentration in the Triton X-100-insoluble fraction was different between these two types of neurons, we next examined lipid distribution in the lipid raft fractions. The lipid raft fractions were isolated as described under "Materials and Methods." The cholesterol concentration in the lipid raft fractions isolated from hippocampal neurons was higher than that from cortical neurons (Fig. 2*e*), whereas there was no significant difference in phospholipid concentration between these two types of neurons in culture (Fig. 2*f*).

Cholesterol Concentration-dependent Regulation of Neurite Outgrowth in Hippocampal and Cortical Neurons—To determine whether a higher cholesterol concentration is responsible for the shorter neurite outgrowth from hippocampal neurons than from cortical neurons, cholesterol concentration in both types of neurons was modulated by treatment with β-cyclodextrin and cholesterol. Interestingly, cholesterol depletion by β-cyclodextrin stimulated neurite outgrowth in hippocampal neurons (Fig. 3, *b* and *d*), which made these neurons similar to cortical neurons without treatment (Fig. 3, *a* and *d*). In contrast, β-cyclodextrin treatment decreased the extent of neurite outgrowth in cortical neurons (Fig. 3, *a* and *c*). Cholesterol loading also decreased the extent of neurite outgrowth in cortical neurons (Fig. 3, *a* and *e*), whereas it had no effects on neurite outgrowth in hippocampal neurons (Fig. 3, *b* and *f*). Neuronal development in cultures has been defined from stages 1 to 5 (26). On the basis of these criteria, we determined the ratio of

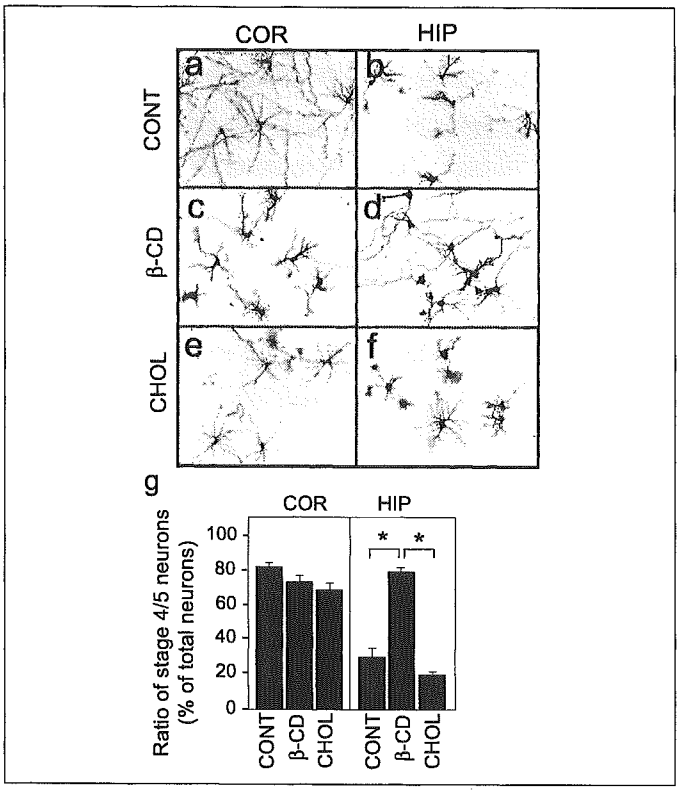

FIGURE 3. **Cholesterol-dependent neurite outgrowth and polarity formation in cortical and hippocampal neurons.** Cortical (*COR*) and hippocampal neurons (*HIP*) were maintained in N_2-medium for 3 days; each culture was treated with β-CD at 5 mM for 10 min, washed in N_2-medium three times, and maintained for another 2 days. Cultures maintained for 3 days were treated with cholesterol (*CHOL*) at 7 μg/ml and maintained for another 2 days. The neurons were then fixed and processed for immunocytochemistry using the anti-tubulin antibody (*a–f*). The ratio of stage 4 and 5 neurons to total neurons in cortical and hippocampal neurons was determined (*g*). The data represent mean ± S.E. For each treatment, 250 neurons were counted. *, $p < 0.0001$. Three independent experiments showed similar results. *CONT*, control.

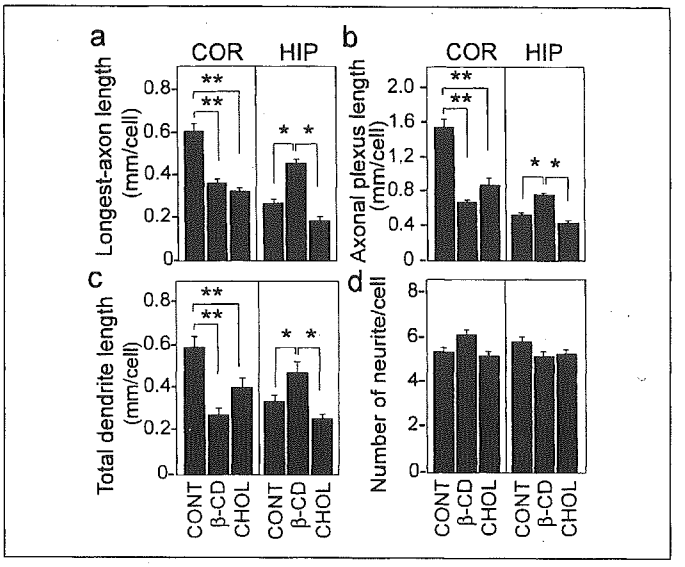

FIGURE 4. **Cholesterol-dependent modulation of axon and dendrite outgrowths in cortical and hippocampal neurons in culture.** Cultured neurons were maintained in N_2-medium for three days after plating, and the cultures were treated with β-CD or cholesterol (*CHOL*) as described in the legend for Fig. 3. The neurons were then immunostained with the anti-tubulin antibody, and longest-axon length (*a*), axonal plexus length (*b*), total dendrite length (*c*), and number of neurites (*d*) per cell were determined. *COR* and *HIP* represent cortical and hippocampal neurons, respectively. The data represent mean ± S.E. Twenty-five neurons were counted for each treatment. *, $p < 0.005$; **, $p < 0.0001$. Three independent experiments showed similar results. *CONT*, control.

neurons at stages 4 and 5 to the total number of neurons. As shown in Fig. 3*g*, cholesterol depletion by β-cyclodextrin treatment or cholesterol loading had no significant effects on the development of cortical neurons (*left panel*). In contrast, β-cyclodextrin treatment stimulated the development of hippocampal neurons; however, cholesterol loading had no significant effects (Fig. 3*g*, *right panel*).

The effects of cholesterol depletion and loading on longest-axon length, axonal plexus length, and total dendrite length of cortical andhippocampal neurons were determined. Cholesterol depletion by treatment with β-cyclodextrin and cholesterol loading decreased the longest-axon length, axonal plexus length, and total dendrite length of cortical neurons (Fig. 4, *a–c*, respectively). In contrast, cholesterol depletion by treatment with β-cyclodextrin increased the longest-axon length, axonal plexus length, and total dendrite length of hippocampal neurons (Fig. 4, *a–c*, respectively), whereas cholesterol loading had no significant effects on these three parameters in hippocampal neurons (Fig. 4, *a–c*). In both types of neurons, these chemicals had no effects on neurite numbers (Fig. 4*d*).

Cholesterol concentrations in cultured neurons treated with β-cyclodextrin or cholesterol loading were determined. Cholesterol concentration in neurons was reduced at 5 h and was recovered at 24 h following treatment with β-cyclodextrin in both cortical and hippocampal neurons (Fig. 5*a*). Cholesterol concentration in neurons increased at 24 h following treatment with cholesterol in both cortical and hippocampal neurons (Fig. 5*a*), although phospholipid concentrations remained unchanged by these treatments (Fig. 5*a*). We further determined the longest-axon length, total dendrite length, and neurite length per cell in cortical and hippocampal neurons treated with β-CD or cholesterol. As shown in Fig. 5*b*, the neurite length was dependent on the treatments.

Fyn, a Member of the Src Family, in Lipid Raft Fraction Is a Key Molecule Modulating Cholesterol-dependent Axon Outgrowth—The observations mentioned above suggest that the difference in cholesterol concentration between cortical and hippocampal neurons could explain differences in neurite outgrowth and neuronal development between these two types of neurons. Because cholesterol concentrations differ in the Triton X-100-insoluble fraction and the lipid raft fraction but not in the Triton X-100-soluble fraction between these two types of neurons (Fig. 2), proteins that are localized in lipid rafts and also play a role in axon and dendrite outgrowths may underlie these differences between cortical and hippocampal neurons in terms of neurite outgrowth. Among the molecules examined, only the level of Fyn in the raft fraction was significantly high in hippocampal neurons treated with β-cyclodextrin, whereas that in total homogenates did not alter (Fig. 6*a*). The levels of flotillin and GM1 did not differ between cortical and hippocampal neurons following these treatments (Fig. 6*a*).

We next determined whether an inhibitor of Fyn signaling, PP2, inhibits the cholesterol deficiency-induced stimulation of axon and dendrite outgrowths in hippocampal neurons. The treatment of hippocampal neurons with 5 μM PP2 inhibited enhanced neurite outgrowth induced by β-cyclodextrin (Fig. 6*b*). However, PP2 did not have any effects on neurite growth in control and cholesterol-loaded neurons (Fig. 6*b*). The neurite outgrowth in hippocampal neurons treated with β-cyclodextrin or cholesterol in the presence or absence of PP2 was quantified. The treatment of hippocampal neurons with PP2 significantly inhibited the increase in longest-axon length and axonal plexus length induced by β-cyclodextrin (Fig. 6*c*, *black bars*); however, PP2 had no effect on neurite outgrowth in control neurons and cholesterol-loaded neurons (Fig. 6*c*, *white bars*). An inhibitory effect of PP2 on the

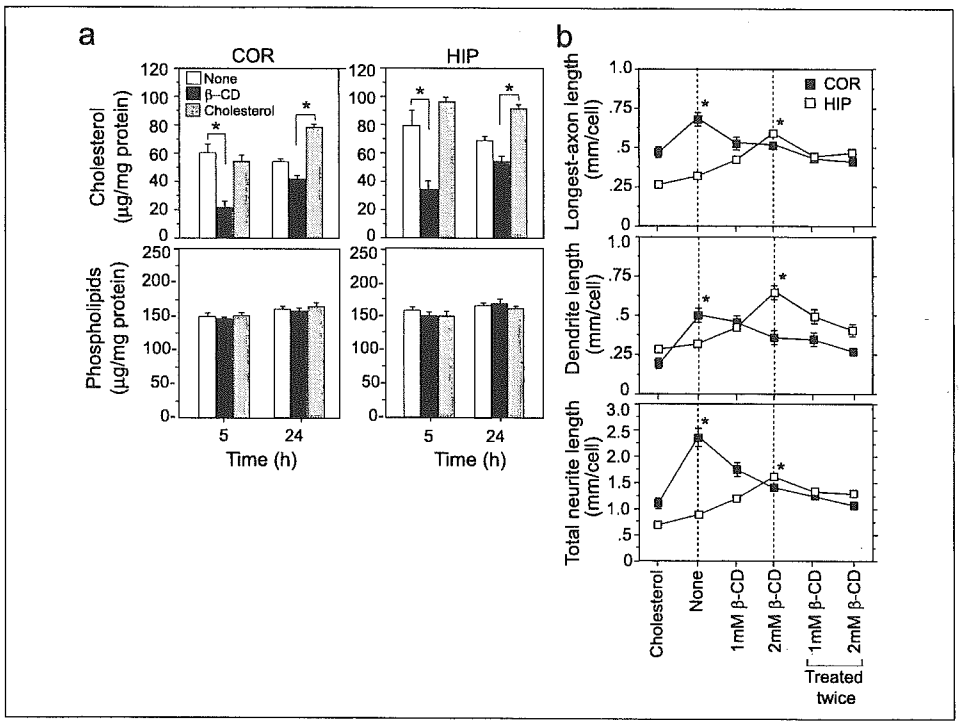

FIGURE 5. **Cholesterol concentrations in hippocampal (*HIP*) and cortical neurons (*COR*) treated with cholesterol and β-cyclodextrin.** Cultured neurons were maintained in N_2-medium for 3 days after plating, and the cultures were treated with β-CD or cholesterol as described in the legend for Fig. 3. *a*, the neurons were then harvested at 5 and 24 h following the treatment, and the concentrations of cholesterol and phospholipids in these cultures were determined as described under "Materials and Methods." The data represent mean ± S.E. Six cultures for each treatment were counted. *, $p < 0.01$. Three independent experiments showed similar results. *b*, cultured neurons maintained in N_2-medium for 3 days after plating were treated with 1 or 2 mM β-CD or 7 μg/ml cholesterol and maintained for another 2 days. Some of the cultures treated with β-CD were treated again with β-CD at the same concentration for 10 min at 37 °C and maintained for 1 additional day. All of the neurons were harvested on culture day 5 and then immunostained with the anti-tubulin antibody. Longest-axon length, total dendrite length, and neurite length per cell were determined. The data represent mean ± S.E. Twenty-five neurons were counted for each treatment. *, $p < 0.005$ *versus* 2 mM β-CD and cholesterol for cortical neurons; *, $p < 0.005$ *versus* cholesterol, no treatment (*None*), and 2 mM β-CD (twice) for hippocampal neurons. Two independent experiments showed similar results.

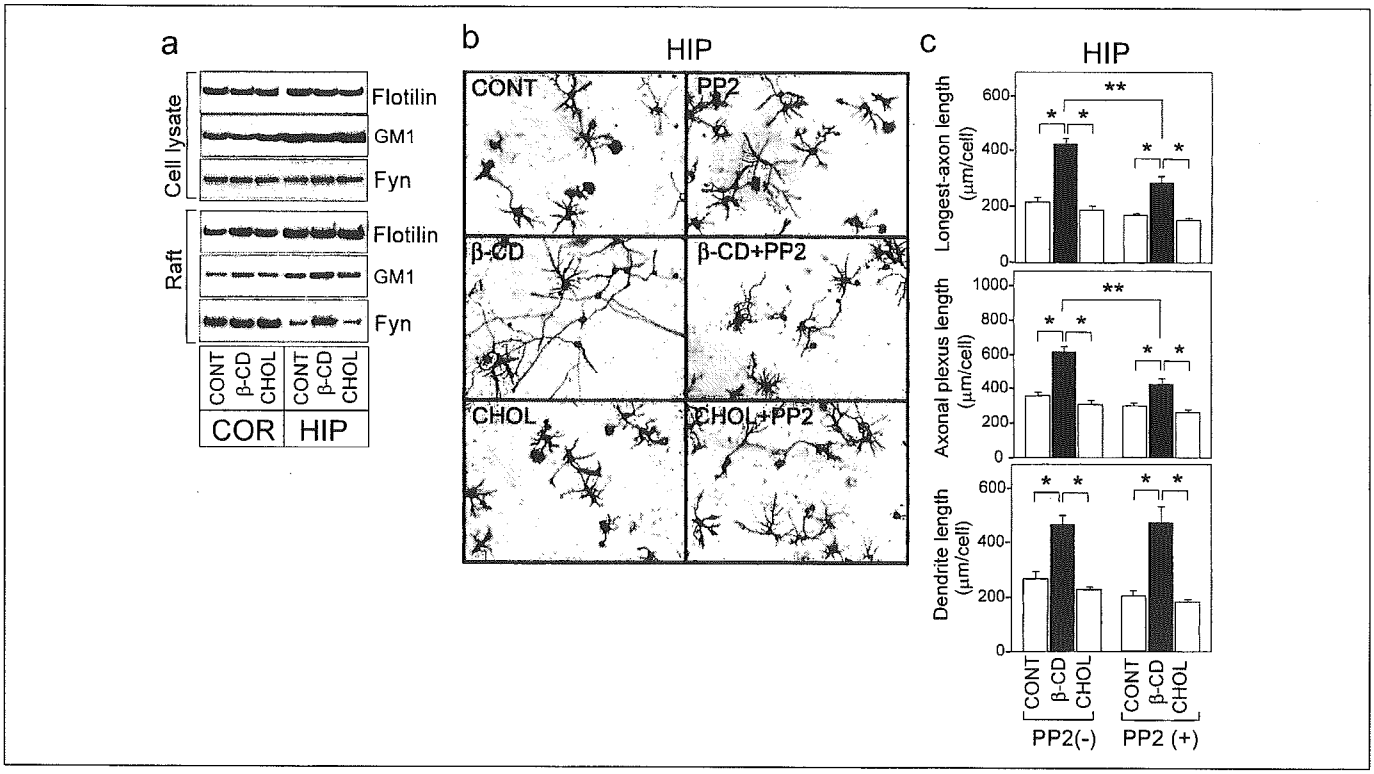

FIGURE 6. **Involvement of Fyn signaling in cholesterol-dependent modulation of axonal outgrowth in hippocampal neurons.** Cortical (*COR*) and hippocampal neurons (*HIP*) were maintained in N_2-medium for 3 days after plating, and the cultures were treated with β-CD or cholesterol (*CHOL*) as described under "Materials and Methods. *a*, the cultures were harvested after 5 days *in vitro*, and each sample was subjected to immunoblot analysis using antibodies specific for flotillin, GM1, and Fyn. *b*, hippocampal neurons were maintained in N_2-medium for 3 days after plating, and the cultures were treated with β-CD or cholesterol as described under "Materials and Methods." The hippocampal neurons were then maintained for another 2 days in the presence or absence of PP2, a Fyn signaling inhibitor, at a concentration of 5 μM. The cultures were then harvested and immunostained. *c*, longest-axon length, axonal plexus length, and dendrite length of the hippocampal neurons not treated (control (*CONT*)) or treated with β-CD or cholesterol in the presence or absence of PP2 were quantified. The data represent mean ± S.E. Twenty-five cells were analyzed for each treatment. *, $p < 0.005$; **, $p < 0.0001$. Three independent experiments showed similar results.

enhanced dendrite outgrowth induced by β-cyclodextrin was not observed (Fig. 6*c*, *bottom panel*).

DISCUSSION

This study showed that cholesterol concentration in hippocampal neurons was markedly higher than in cortical neurons and that the neurite outgrowth was significantly greater and the polarity formation occurred earlier in cortical neurons than in hippocampal neurons. In contrast, the phospholipid concentrations in these neurons were similar. Our finding that the cholesterol biosynthetic pathway is highly enhanced in hippocampal neurons compared with cortical neurons (supplemental Fig. S2) may explain the difference in cholesterol concentration between these two types of neurons.

Cholesterol depletion from hippocampal neurons markedly enhanced axon and dendrite outgrowth and accelerated the establishment of cell polarity. The morphological features appeared similar to those in cortical neurons, suggesting that a high concentration of cholesterol attenuates neurite outgrowth and polarity formation in hippocampal neurons in culture. The finding that both the loading of cholesterol to and the depletion of cholesterol from the cortical neurons attenuated neurite outgrowth suggests that there may be an optimal concentration of cholesterol for cortical neurons to exhibit neurite outgrowth (Figs. 3 and 4). This is also the case for hippocampal neurons, because the neurite outgrowth was inhibited when cholesterol was further depleted from cultured neurons by treatment with β-CD twice (Fig. 5*b*).

The cholesterol concentration in the Triton X-100-insoluble fraction from hippocampal neurons was greater than that from cortical neurons, whereas cholesterol concentration in the Triton X-100-soluble fraction did not differ between these two types of neurons, indicating that the difference in the concentration of cholesterol in the Triton X-100-insoluble fraction may explain the neuron-specific difference in total cholesterol concentration between these two types of neurons. This notion is supported by the finding that cholesterol concentration in lipid rafts isolated from hippocampal neurons is higher than in those from cortical neurons (Fig. 2). In contrast to cholesterol concentration, phospholipid concentration did not show any difference between these two types of neurons. This also suggests that neuronal differentiation and neurite outgrowth in hippocampal neurons may be modulated by cholesterol in lipid rafts and raft-localized molecules and that the morphological difference between cortical and hippocampal neurons can be explained by the difference in cholesterol concentration between these neurons.

The mechanism by which a decreased level of cholesterol in lipid rafts modulates neurite outgrowth has not been completely understood. However, the finding that the enhancement of neurite outgrowth induced by β-cyclodextrin treatment is accompanied by the recruitment of Fyn to lipid rafts and that the Src family inhibitor PP2 inhibits axonal elongation induced by β-cyclodextrin treatment suggests that an increased level of raft-localized Fyn is in part involved in β-cyclodextrin-induced axonal elongation in hippocampal neurons. This notion is supported by previous studies showing that Src family kinases, including Fyn, play a critical role in axon outgrowth (27, 28) and that lipid raft-localized Fyn is more catabolically active than non-raft-localized Fyn (29, 30).

Another interesting point is that cellular cholesterol concentration modulates the development of hippocampal neurons but not that of cortical neurons (Fig. 3), although it modulates neurite outgrowth in both types of neurons (Figs. 4 and 5). As demonstrated previously (26), neurons initially establish several apparently identical, short processes. With culture time, one of the processes begins to grow very rapidly and becomes an axon, and the other processes then become dendrites. Interestingly, the establishment of neuronal polarity in hippocampal neurons depends on cellular cholesterol concentration; a decreased cholesterol concentration stimulates the establishment of neuronal polarity, whereas an increased concentration of cellular cholesterol inhibits it. This is not the case for cortical neurons. The present study does not provide any explanation for the discrepancy in the cell type-specific regulation of polarity formation mediated by cholesterol. This may suggest that cholesterol is not the only lipid responsible for the observed alterations and that membrane composition is relevant for cortical neurons. Further study is required to clarify the mechanism underlying the cell type-specific regulation of polarity formation mediated by cholesterol.

Recent studies have shown that cholesterol supplied as an apoE-lipoprotein complex to neurons via apoE receptors plays a critical role in synaptogenesis, neurite outgrowth, and neuronal repair (9–11). Most of the published literature is concerned with only a single neuronal subtype, which is not sufficient for the appreciation of the complex role of cholesterol in neurons. The present study shows that cholesterol demand and the optimal cholesterol concentration for neurite outgrowth depend completely on the neuronal type and that the mechanism underlying the effect of cholesterol on neuronal maturation involves the attainment of the optimal cholesterol concentration. There are issues that need to be elucidated to delineate the mechanisms underlying the neuronal type-specific regulation of neurite outgrowth by cellular cholesterol concentration, and it is required to confirm that the present findings are also the case *in vivo*. However, the present study suggests that the role of cholesterol in relation to neuronal phenotypes and functions should be elucidated in a neuron type- and brain region-specific manner.

REFERENCES

1. Schwarz, A., Rapaport, E., Hirschberg, K., and Futerman, A. H. (1995) *J. Biol. Chem.* **270,** 10990–10998
2. Ledesma, M. D., Simons, K., and Dotti, C. G. (1998) *Proc. Natl. Acad. Sci. U. S. A.* **95,** 3966–3971
3. Ledesma, M. D., Brugger, B., Bunning, C., Wieland, F. T., and Dotti, C. G. (1999) *EMBO J.* **18,** 1761–1771
4. Simons, K., and Toomre, D. (2000) *Nat. Rev. Mol. Cell Biol.* **1,** 31–39
5. Fan, Q.-W., Yu, W., Gong, J. S., Zou, K., Sawamura, N., Senda, T., Yanagisawa, K., and Michikawa, M. (2002) *J. Neurochem.* **80,** 178–190
6. Fan, Q. W., Yu, W., Senda, T., Yanagisawa, K., and Michikawa, M. (2001) *J. Neurochem.* **76,** 391–400
7. Goodrum, J. F., Brown, J. C., Fowler, K. A., and Bouldin, T. W. (2000) *J. Neuropathol. Exp. Neurol.* **59,** 1002–1010
8. Karten, B., Vance, D. E., Campenot, R. B., and Vance, J. E. (2003) *J. Biol. Chem.* **278,** 4168–4175
9. Hayashi, H., Campenot, R. B., Vance, D. E., and Vance, J. E. (2004) *J. Biol. Chem.* **279,** 14009–14015
10. Mauch, D. H., Nagler, K., Schumacher, S., Goritz, C., Muller, E. C., Otto, A., and Pfrieger, F. W. (2001) *Science* **294,** 1354–1357
11. Koudinov, A. R., and Koudinova, N. V. (2001) *FASEB J.* **15,** 1858–1860
12. Braak, H., and Braak, E. (1997) *Neurobiol. Aging* **18,** 351–357
13. Price, J. L., and Morris, J. C. (1999) *Ann. Neurol.* **45,** 358–368
14. Katsuno, T., Morishima-Kawashima, M., Saito, Y., Yamanouchi, H., Ishiura, S., Murayama, S., and Ihara, Y. (2005) *Neurology* **64,** 687–692
15. Simons, M., Keller, P., Dichgans, J., and Schulz, J. B. (2001) *Neurology* **57,** 1089–1093
16. Simons, M., Keller, P., De Strooper, B., Beyreuther, K., Dotti, C. G., and Simons, K. (1998) *Proc. Natl. Acad. Sci. U. S. A.* **95,** 6460–6464
17. Fassbender, K., Simons, M., Bergmann, C., Stroick, M., Lutjohann, D., Keller, P., Runz, H., Kuhl, S., Bertsch, T., von Bergmann, K., Hennerici, M., Beyreuther, K., and Hartmann, T. (2001) *Proc. Natl. Acad. Sci. U. S. A.* **98,** 5856–5861
18. Sawamura, N., Gong, J. S., Garver, W. S., Heidenreich, R. A., Ninomiya, H., Ohno, K., Yanagisawa, K., and Michikawa, M. (2001) *J. Biol. Chem.* **276,** 10314–10319
19. Bu, B., Li, J., Davies, P., and Vincent, I. (2002) *J. Neurosci.* **22,** 6515–6525
20. Suzuki, K., Parker, C. C., Pentchev, P. G., Katz, D., Ghetti, B., D'Agostino, A. N., and

Carstea, E. D. (1995) *Acta Neuropathol. (Berl.)* **89,** 227–238
21. Michikawa, M., and Yanagisawa, K. (1999) *J. Neurochem.* **72,** 2278–2285
22. Yu, W., Gong, J. S., Ko, M., Garver, W. S., Yanagisawa, K., and Michikawa, M. (2005) *J. Biol. Chem.* **280,** 11731–11739
23. Gong, J. S., Kobayashi, M., Hayashi, H., Zou, K., Sawamura, N., Fujita, S. C., Yanagisawa, K., and Michikawa, M. (2002) *J. Biol. Chem.* **277,** 29919–29926
24. Lisanti, M. P., Scherer, P. E., Vidugiriene, J., Tang, Z., Hermanowski-Vosatka, A., Tu, Y. H., Cook, R. F., and Sargiacomo, M. (1994) *J. Cell Biol.* **126,** 111–126
25. Sawamura, N., Ko, M., Yu, W., Zou, K., Hanada, K., Suzuki, T., Gong, J. S., Yanagisawa, K., and Michikawa, M. (2004) *J. Biol. Chem.* **279,** 11984–11991
26. Dotti, C. G., Sullivan, C. A., and Banker, G. A. (1988) *J. Neurosci.* **8,** 1454–1468
27. Meriane, M., Tcherkezian, J., Webber, C. A., Danek, E. I., Triki, I., McFarlane, S., Bloch-Gallego, E., and Lamarche-Vane, N. (2004) *J. Cell Biol.* **167,** 687–698
28. Liu, G., Beggs, H., Jurgensen, C., Park, H. T., Tang, H., Gorski, J., Jones, K. R., Reichardt, L. F., Wu, J., and Rao, Y. (2004) *Nat. Neurosci.* **7,** 1222–1232
29. Mukherjee, A., Arnaud, L., and Cooper, J. A. (2003) *J. Biol. Chem.* **278,** 40806–40814
30. Shima, T., Nada, S., and Okada, M. (2003) *Proc. Natl. Acad. Sci. U. S. A.* **100,** 14897–14902

THE JOURNAL OF BIOLOGICAL CHEMISTRY

Vol. 280, No. 29, Issue of July 22, pp. 27296–27302, 2005
Printed in U.S.A.

Neurodegeneration in Heterozygous Niemann-Pick Type C1 (NPC1) Mouse

IMPLICATION OF HETEROZYGOUS NPC1 MUTATIONS BEING A RISK FOR TAUOPATHY*

Received for publication, April 11, 2005, and in revised form, May 18, 2005
Published, JBC Papers in Press, May 25, 2005, DOI 10.1074/jbc.M503922200

Wenxin Yu, Mihee Ko, Katsuhiko Yanagisawa, and Makoto Michikawa‡

From the Department of Alzheimer's Disease Research, National Institute for Longevity Sciences, 36-3 Gengo, Morioka, Obu, Aichi 474-8522, Japan

Niemann-Pick type C1 (NPC1) disease is an autosomal recessive, fatal disorder characterized by a defect in cholesterol trafficking and progressive neurodegeneration. The disease is predominantly caused by mutations in the *NPC1* gene; however, it has been assumed that heterozygous *NPC1* mutations do not cause any symptoms. Here we demonstrate that cholesterol accumulation does not occur in young mouse brains; however, it does in aged (104–106-week-old) NPC1+/− mouse brains. In addition, Purkinje cell loss was observed in aged NPC1+/− mouse cerebellums. Immunoblot analysis using anti-phospho-tau antibodies (AT-8, AT-100, AT-180, AT-270, PHF-1, and SMI-31) demonstrates the site-specific phosphorylation of tau at Ser-199, Ser-202, Ser-212, and Thr-214 in the brains of aged NPC1+/− mice. Mitogen-activated protein kinase, a potential serine kinase known to phosphorylate tau, was activated, whereas other serine kinases, including glycogen synthase kinase 3β, cyclin-dependent kinase 5, or stress-activated protein kinase/c-Jun N-terminal kinase were not activated. Cholesterol level in the lipid raft isolated from the cerebral cortices, ATP level, and ATP synthase activity in the cerebral cortices significantly decreased in the aged NPC1+/− brains compared with those in the NPC1+/+ brains. All of these changes observed in NPC1+/− brains were determined to be associated with aging and were not observed in the age-matched NPC1+/+ brains. These results clearly demonstrate that heterozygous NPC1 impairs neuronal functions and causes neurodegeneration in aged mouse brains, suggesting that human heterozygous NPC1 mutations may be a risk factor for neurodegenerative disorders, such as tauopathy, in the aged population.

Niemann-Pick type C1 (NPC1)[1] disease is an autosomal recessive disorder characterized by progressive neurodegeneration including ataxia, dystonia, seizures, and dementia (1). In NPC1-deficient cells, exogenously transported and endogenously synthesized cholesterol accumulate in late endosome/lysosomes, with delayed cholesterol transport to cellular compartments responsible for the regulation of intracellular cholesterol homeostasis (2–5). In addition to cholesterol, glycosphingolipids and other lipids accumulate in homozygous NPC1 brains with aging (1, 6). The gene responsible for NPC1 disease, *NPC1*, was cloned in both humans and mice (7, 8). It was previously demonstrated that NPC1 plays a key role in the transport of cholesterol to the *trans*-Golgi network, plasma membrane, and endoplasmic reticulum (9–12).

The neuropathological features of NPC1 brains are characterized by the loss of neurons such as Purkinje cells, hyperphosphorylated tau, and neurofibrillary tangle formation with the accumulation of lipid storage bodies and the presence of dendritic and axonal abnormalities (6, 13–16). These lines of evidence suggest that the intracellular accumulation of cholesterol and gangliosides correlates with the progression of NPC1 disease and induces neurodegeneration. However, there is a different viewpoint on the pathogenesis of NPC1 disease; *i.e.* the continuous defective use of cholesterol in NPC1 neural tissues causes tauopathy (6, 16, 17). This notion is supported by previous studies showing that there is cholesterol deficiency in cellular compartments including distal axons (18), although cholesterol accumulation occurs in the late endosome/lysosomal compartment (4, 5) due to a defect in the transport of cholesterol, the source of which is either endogenous synthesis or exogenous uptake.

With respect to neuronal gangliosides, a previous study supports the notion that the accumulation of gangliosides causes neurodegeneration (19), whereas another study indicates that the accumulation of gangliosides is not the cause of neurodegeneration in NPC1 mice (20). A recent study has demonstrated that impaired neurosteroidogenesis, due to disordered cholesterol trafficking, affects neuronal growth and differentiation and that allopregnanolone treatment delays the onset of neurological symptoms and lengthens the life of NPC1 mice (21).

Our recent study has shown a novel mechanism underlying neurodegeneration in NPC1 disease, whereby an increased cholesterol level in mitochondrial membranes adversely affects mitochondrial membrane potential, the synthesis of ATP, and the level of cellular ATP in NPC1 mouse brains and neurons (22). Since mitochondria are a key organelle for steroidogenesis, mitochondrial dysfunction may responsible for impaired neurosteroidogenesis. In addition, this also indicates that not whole-cell cholesterol level but rather compartment- or organelle-associated cholesterol level is critical for maintaining neuronal functions.

* This work was supported by grants from the Ministry of Health, Labor, and Welfare of Japan (Comprehensive Research on Aging and Health Grant H14-10 and Research on Human Genome and Tissue Engineering Grant H17-004), by the Pharmaceuticals and Medical Devices Agency, Japan, and by the National Niemann-Pick Disease Foundation, USA. The costs of publication of this article were defrayed in part by the payment of page charges. This article must therefore be hereby marked "*advertisement*" in accordance with 18 U.S.C. Section 1734 solely to indicate this fact.

‡ To whom correspondence should be addressed. Tel.: 81-562-46-2311; Fax: 81-562-46-3157; E-mail: michi@nils.go.jp.

[1] The abbreviations used are: NPC1, Niemann-Pick type C1; MAPK, mitogen-activated protein kinase; ERK, extracellular signal-regulated kinase; GSK-3β, glycogen synthase kinase 3β; SAPK, stress-activated protein kinase; JNK, c-Jun N-terminal kinases; Cdk5, cyclin-dependent kinase 5; PBS, phosphate-buffered saline; GM1, Galβ1-3Gal-NAcβ1-4Gal(3-2αNeuAc)β1-4Glcβ1-1Cer.

Note that NPC1 disease is an autosomal recessive disease, and heterozygous carriers of NPC1 mutations are not assumed to develop any neurological symptoms during their entire life span, and note that the effect of heterozygous NPC1 mutations on the development of neurological disorders has not been extensively investigated. This is also the case for NPC1+/− mice. However, intermediate abnormalities in terms of cholesterol metabolism have been shown in nonneuronal cells from NPC1 patients (23–25) and in nonneuronal tissues or cells from NPC1+/− mice (26–28). In addition, our recent study has demonstrated that NPC1+/− exhibits intermediate dysfunction in the mitochondria of the brains of NPC1+/− mice at 9 weeks of age (22). These lines of evidence have led us to examine whether there occurs neuronal dysfunction or damage in NPC1+/− mouse brains under certain conditions such as aging.

In this study, morphological and biochemical studies were performed on brains of aged heterozygous NPC1+/− mice. In contrast to what has been assumed, neurodegeneration as demonstrated by Purkinje cell loss, enhanced phosphorylation of tau, and activated MAPK/ERK1/2 were clearly observed in NPC1+/− mouse brains. It has been assumed that mutant NPC1 heterozygotes do not develop any clinical symptoms; however, these results suggest that heterozygous NPC1 mutations may be a risk factor for tauopathy. Since it is estimated that the incidence of NPC1 disease is as high as 1:150,000 (1), the percentage of the total population with the heterozygous NPC1 mutation is estimated to be around 0.5%. Thus, our present results show that heterozygous NPC1 mutations unexpectedly affect brains with aging and thus may lead to the investigation of the link between heterozygous NPC1 mutations and neurodegenerative diseases, such as Alzheimer disease.

EXPERIMENTAL PROCEDURES

BALB/c NPC1NIH Mice—The animal care and experiments using animals performed in this study were carried out in accordance with institutional guidelines. BALB/c mice carrying the genetic mutation for NPC1 were obtained from The Jackson Laboratory (Bar Harbor, ME). These heterozygous mice were bred to acquire NPC1+/+ and NPC1+/− mice used in this study. The genotypes of the mice were determined from genomic DNA isolated from tail snip DNA using a PCR-based method and oligonucleotide primers described previously (7). PCR products were separated using a 1.2% agarose gel. The mice used in this study ranged from 104 to 106 weeks of age.

Reagents—The monoclonal anti-phospho-independent tau antibody T46 was obtained from Zymed Laboratories, Inc. (South San Francisco, CA). The monoclonal anti-tau antibodies AT8 (specific for phospho-Ser^{199} and -Ser^{202}), AT-100 (specific for phospho-Ser^{212} and -Thr^{214}), AT180 (specific for phospho-Thr^{231}), and AT-270 (specific for phospho-Thr^{181}) were purchased from Innogenetics (Ghent, Belgium). The monoclonal anti-tau antibody SMI31 (specific for phospho-Ser^{396}) was purchased from Sternberger Monoclonals Inc. (Baltimore, MD). The monoclonal anti-tau antibody, PHF-1 (specific for phospho-Ser^{396} and -Ser^{404}), was kindly provided by Dr. P. Davies (Albert Einstein College of Medicine). Rabbit polyclonal antibodies specific for phospho-MAPK/ERK1/2 (specific for phospho-Thr^{202} and -Tyr^{204}), pan-MAPK/ERK1/2, phospho-SAPK/JNK, and pan-SAPK/JNK and a monoclonal antibody recognizing phospho-GSK-3β (specific for phospho-Tyr^{279} and -Tyr^{216}) were purchased from Cell Signaling Technology (Beverly, MA). The monoclonal anti-phospho-independent GSK-3β antibody was purchased from BD Transduction Laboratories (Lexington, KY). The rabbit anti-p35 antibody, which reacts with the p35 and p25 regulatory subunits of cyclin-dependent kinase 5 (Cdk5), was obtained from Santa Cruz Biotechnology, Inc. (Santa Cruz, CA). The polyclonal anti-calbindin D28K was obtained from Chemicon International (Temecula, CA). The monoclonal anti-flotillin-1 antibody and anti-β-tubulin antibody were purchased from Covance (Richmond, CA) and BD Transduction Laboratories (San Jose, CA), respectively. Horseradish peroxidase-conjugated cholera toxin B and the filipin complex were purchased from Sigma.

Histological Analysis—The mice were sacrificed by CO_2 inhalation and perfused intracardially with 0.1 M phosphate-buffered saline (PBS) containing heparin (50 units/ml). The brains were removed and fixed in 4% paraformaldehyde in PBS overnight at 4 °C and then rinsed with PBS and cryoprotected in a solution of 30% sucrose in PBS. Fixed tissues were sectioned on a semimotorized rotary microtome (LEICA RM2145, Wetzlar, Germany) at 30 μm and processed for immunohistochemistry with the anti-calbindin D28K (1:500) and AT8 (1:500). Immunoreactivity was detected with diaminobenzidine using the ABC Elite kit according to the manufacturer's instructions (Vector Laboratories, Burlingame, CA). For cresyl violet staining, slides were immersed in 70, 80, and 95%, ethanol for 5 min each and in 100% ethanol for 5 min and then in xylene for 15 min. The slides were then sequentially immersed back in 100, 95, and 70% ethanol solutions and distilled water for 5 min in each. The slides were stained for 1 min in filtered cresyl violet solution and then briefly rinsed twice in distilled water. They were then sequentially dehydrated again in 70, 80, 95, and 100% ethanol solutions for 2 min each. The slides were placed in xylene for another 10 min and then mounted with Permount. For double fluorescence staining, the sections were treated overnight with calbindin D28K antibody (1:500) and AT-8 antibody (1:500) at 4 °C overnight, followed by incubation with second antibodies, rhodamine-conjugated goat anti-rabbit IgG (Chemicon International, Temecura, CA) diluted at 1:500, and fluorescein isothiocyanate-conjugated goat anti-mouse IgG (American Qualex, San Clemente, CA) diluted at 1:50, for 1 h at room temperature. The slides were then washed with PBS and mounted with Vectashield (Vector). For costaining with calbindin D28K antibody and filipin, the sections were incubated overnight with calbindin D28K antibody (1:500) at 4 °C overnight, followed by washing three times for 5 min each using 100 μg/ml filipin in PBS and then incubated with rhodamine-conjugated goat anti-rabbit IgG (1:500) for 1 h at room temperature. The slides were then washed with PBS and mounted with Vectashield (Vector). Fluorescent images were obtained using a model LSM 510 laser-scanning confocal microscope (Zeiss) equipped with a × 63 Plan Apochromat numerical aperture and a 1.4 oil immersion objective.

Protein Preparation—The mice were sacrificed by CO_2 inhalation, and their brains were harvested, rinsed in PBS, and immediately frozen in liquid nitrogen. The cerebrum and cerebellum were separated and homogenized in 10 volumes of Tris-saline (50 mM Tris-HCl (pH 7.4) and 150 mM NaCl), containing protease inhibitors (Complete™) and phosphatase inhibitors (10 μM NaF and 1 mM orthovanadate) using a motor-driven Teflon homogenizer. The homogenates were centrifuged at 3,000 × *g* for 10 min at 4 °C, and the supernatants were stored for biochemical analyses. Protein concentration was determined using the bicinchoninic acid protein assay kit (Pierce).

Determination of ATP Level—ATP level in mouse brain tissues was determined as previously reported (22). In brief, the homogenates of cerebrum and cerebellum were centrifuged at 10,000 rpm for 2 min at 4 °C and then rinsed three times with PBS. ATP level in these samples was determined using the ATP Bioluminescence Assay kit CLS II (Roche Applied Science). In brief, the pellet was resuspended in 50 μl of ice-cold ATP lysis buffer (100 mM Tris and 4 mM EDTA, pH 7.75), to which 150 μl of boiling ATP lysis buffer was added, and the samples were incubated for 2 min at 99 °C. The samples were centrifuged at 10,000 rpm for 1 min at 4 °C, and the supernatants were collected. Finally, the ATP level was determined by combining 50 μl of the supernatant with 50 μl of the luciferase reagent. After a 20-s delay, chemiluminescence was measured with a 2.6-s integration time using a microplate luminometer (EG&G Berthold, Bad Wildbad, Germany). Luciferase activity was expressed in fluorescence units/μg of protein.

Determination of ATP Synthase Activity—Brain mitochondria were isolated as previously reported (22). For the determination of ATP synthase activity, 100 μg of mitochondrial protein from each sample was used to measure the rate of ATP synthesized. The reaction was initiated by adding 100 μg of mitochondrial protein into 100 μl of reaction buffer (10 mM K_2HPO_4 (pH 7.4) 300 mM D-mannitol, 10 mM KCl, and 5 mM $MgCl_2$) at 37 °C. After 1 min, 10 μl of ADP (50 μM) was added, and the intensity of bioluminescence was recorded at 37 °C, where peak height was proportional to the amount of ATP synthesized.

Immunoblot Analysis—Equal amounts of proteins separated using 4–20% gradient Tris/Tricine SDS–PAGE (Dai-ichi Pure Chemical Co., Ltd., Tokyo, Japan) were electrophoretically transferred onto a polyvinylidene difluoride membrane (Millipore Corp., Bedford, MA). Nonspecific binding was blocked with 5% fat-free milk in phosphate-buffered saline containing 0.1% Tween 20. The blots were then incubated with primary antibodies overnight at 4 °C. For the detection of both monoclonal and polyclonal antibodies, appropriate peroxidase-conjugated secondary antibodies were used in conjunction with SuperSignal chemiluminescence (Pierce) to obtain images on the film.

Preparation of Raft Fractions—Detergent-insoluble membrane raft fractions were obtained according to the established method previously

reported (6). One milliliter of each fraction was sequentially collected from the top of the gradient. The extraction of lipids and the subsequent determination of the amounts of cholesterol and phospholipids in each sample were carried out according to previously described methods (29).

Lipid Analysis—The levels of cholesterol and phospholipids in the samples were determined using enzymatic methods. Cholesterol level was determined using a cholesterol determination kit, LTCII (Kyowa Medex, Tokyo), whereas phospholipid level was determined using a phospholipid determination kit, PLB (Wako, Osaka, Japan).

Detection of GM1 Ganglioside—For the detection of GM1 ganglioside, samples from each fraction were dissolved in equal volumes of Laemmli buffer. They were then subjected to 4–20% gradient Tris/Tricine SDS-PAGE (Dai-ichi Pure Chemical Co., Ltd.). The separated GM1 ganglioside was transferred onto an Immobilon or polyvinylidene difluoride membrane (Millipore) with a semidry electrophoretic transfer apparatus (Nihon Eido, Tokyo, Japan) using a transfer buffer (0.1 M Tris, 0.192 M glycine, and 20% methanol). The membranes were blocked with 5% fat-free milk in PBS containing 0.1% Tween 20 for 1 h and probed with horseradish peroxidase-conjugated cholera toxin B (Sigma) (final concentration of 42 ng/ml) overnight at 4 °C. In between steps, the membranes were washed four times with PBS-T for 15 min. Bound cholera toxin was detected using Super Signal Chemiluminescence (Pierce).

Statistical Analysis—Statistical analysis was carried out using StatView computer software (Macintosh version 5.0, Abacus Concepts Inc., Berkeley, CA). A p value of <0.05 was considered to be significant.

RESULTS

Cholesterol Accumulation in Brains of Aged NPC1 Heterozygous Mouse—The brains of NPC1+/+ and NPC1+/− mice at 24, 40, and 104–106 weeks of age were isolated, and the levels of cholesterol and phospholipids were determined. The cholesterol levels in the cerebrum and cerebellum of the NPC1+/− mice were significantly elevated compared with those in the same brain areas of the NPC1+/+ mice at 104–106 weeks of age (Fig. 1*a*), whereas the cholesterol levels were similar in the two groups at 24 and 40 weeks of age (Fig. 1*a*). The phospholipid levels were similar in the two genotypes at every age examined (Fig. 1*b*). The filipin and calbindin staining of brain samples (the third lobe of each cerebellum) prepared from the NPC1+/+ and NPC1+/− mice at 104 weeks of age shows that cells exhibiting a strong filipin-positive signal in the NPC1+/− cerebellar section (from the third lobe) are also calbindin-positive, whereas the calbindin-positive cells in the NPC1+/+ cerebellar section exhibit a very weak signal for filipin staining (Fig. 1*c*). These results indicate that cholesterol accumulation occurs in Purkinje cells of aged NPC1+/− mouse cerebellum.

Purkinje Cell Loss in Aged NPC1 Heterozygous Mice—The cerebellums of NPC1+/+ and NPC1+/− mice at 104–106 weeks of age were immunohistochemically analyzed using the anti-calbindin antibody, which specifically recognizes Purkinje cells. The number of anti-calbindin antibody-positive cells decreased in the NPC1+/− cerebrum (Fig. 2, *d–f*) compared with that in the NPC1+/+ cerebellum (Fig. 2, *a–c*), suggesting that Purkinje cell loss occurred in the aged NPC1+/− cerebellum. However, this was not the case for the NPC1+/− cerebellum at 24 and 40 weeks of age (data not shown). Next, the number of anti-calbindin antibody-positive cells in each lobe of the cerebellums of the NPC1+/+ and NPC1+/− mice at 104–106 weeks of age was determined. The number of Purkinje cells was significantly decreased in first + second, third, seventh, and eighth lobes of NPC1+/− cerebellum compared with those of NPC1+/+ cerebellum (Fig. 2*g*).

Hyperphosphorylation of Tau in NPC1+/− Mouse Brain—Since neurodegeneration found in the NPC homozygous mouse brain is accompanied by hyperphosphorylated tau (6, 16), the sagittal sections of the brains were immunohistochemically stained using the anti-phospho-tau antibody AT-8. AT-8 stained neurons strongly in the cerebral cortices and hippocampus of the NPC1+/− mice (Fig. 3, *b* and *d*) compared with those of the NPC1+/+ mice (Fig. 3, *a* and *c*). For cerebellar sections,

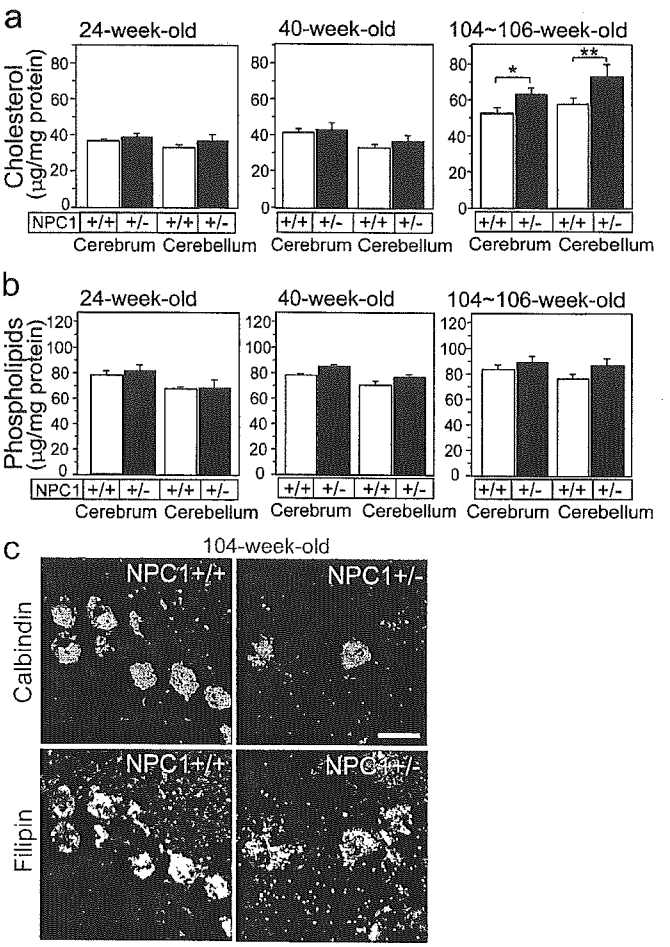

FIG. 1. **Cholesterol accumulation in aged NPC1+/− mouse brains.** Cholesterol and phospholipids were extracted from the brains of the NPC1+/+ and NPC1+/− mice at 24, 40, and 104–106 weeks of age, and their levels were determined. The levels of cholesterol (*a*) and phospholipids (*b*) per mg of protein are shown. *, $p < 0.04$; **, $p < 0.01$. The results represent the mean ± S.E. of three different samples and are representative of three independent experiments. *c*, brain sections from the third lobes of each cerebellum of NPC1+/+ and NPC1+/− mice at 104 weeks old were subjected to filipin and calbindin staining as described under "Experimental Procedures" and visualized using confocal laser microscopy. Purkinje neurons demonstrated as calbindin-positive cells in NPC1+/− mouse cerebellum were strongly stained with filipin, whereas those in NPC1+/+ mouse cerebellum were only weakly stained. *Scale bar*, 25 μm.

double staining using anti-calbindin antibody was performed. The Purkinje cells demonstrated as being calbindin-positive were very faintly stained with AT-8 in the aged NPC1+/− mouse cerebellum, whereas calbindin-positive Purkinje cells were also AT-8-positive in the aged NPC1+/+ mouse cerebellum (Fig. 3, *e–h*). The ratio of AT-8-positive Purkinje cells to total Purkinje cells was very high in NPC1+/− mouse cerebella compared with that of NPC1+/+ mouse cerebella (Fig. 3*i*).

To verify that the histologic abnormalities are a result of enhanced tau phosphorylation, immunoblot analysis was conducted using lysates of the NPC1+/+ and NPC1+/− cerebrums and cerebellums. The antibodies used were T-46, which recognizes phospho-independent tau; AT-8, AT-100, AT-180, AT-270, PHF-1, and SMI-31, which recognize site-specific phosphorylation of tau; and the anti-β-tubulin antibody as an internal standard. The intensities of the signals corresponding to phosphorylated tau demonstrated by AT-8 and AT-100 increased in the cerebrum and cerebellum of the NPC1+/− mice at 104–106 weeks of age compared with those for the NPC1+/+ mice of at the same age (Fig. 4*a*). However, the intensities of the signals

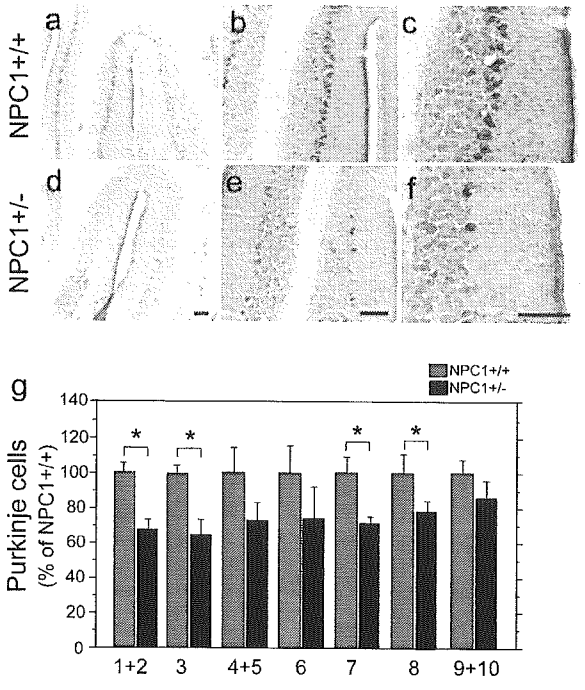

FIG. 2. **Cerebellar histology in aged NPC1+/− mouse brains.** Brain sections (cerebellum) from the NPC1+/+ and NPC1+/− mice at 104–106 weeks old were subjected to immunohistochemistry using the anti-calbindin antibody D28, as described under "Experimental Procedures." Calbindin-immunoreactive neurons in the third lobes of the cerebellum of NPC1+/+ (*a–c*) and NPC1+/− (*d–f*) are shown on different scales. *Scale bars*, 100 μm. *g*, the number of calbindin-immunopositive neurons was determined in all of the cerebellar lobes of the NPC1+/+ and NPC1+/− mice. 20 sections prepared from the NPC1+/+ and NPC1+/− mice were counted. Each section contained 489 ± 45 Purkinje cells for the NPC1+/+ cerebellum and 346 ± 24 Purkinje cells for the NPC1+/− cerebellum. Data are presented as a percentage of the number of Purkinje neurons in the NPC1+/+ mice (n = 5 for each genotype). *, $p < 0.05$.

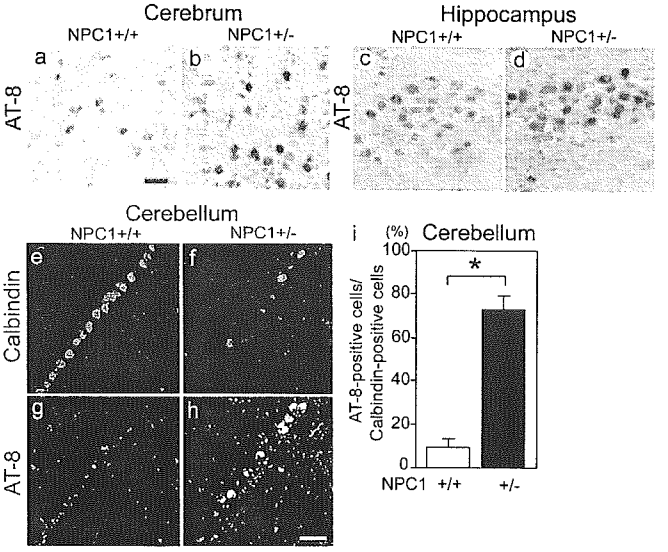

FIG. 3. **Immunohistochemical analysis of cerebral, hippocampal, and cerebellar sections of 104–106-week-old NPC1+/+ and NPC1+/− mice.** *a–d*, cerebral and hippocampal sections were subjected to immunohistochemical analysis using the phospho-tau antibody AT-8, as described under "Experimental Procedures," and visualized with diaminobenzidine using the ABC Elite kit. *e–h*, for cerebellar sections, double staining using AT-8 and anti-calbindin antibody was performed. AT-8-positive neurons were visualized with fluorescein isothiocyanate-conjugated second antibody, and calbindin-positive neurons were visualized with rhodamine-conjugated second antibody. *i*, the numbers of AT-8-positive cells in 50 calbindin-positive cells were counted, and the ratio of AT-8-positive cells to calbindin-positive cells was calculated. Data represent the mean ± S.E. of six samples. *, $p < 0.001$. *Scale bar*, 50 μm.

demonstrated by AT-180, AT-270, PHF-1, and SMI-31 did not differ between samples from the NPC1+/+ and NPC1+/− brains (Fig. 4*a*). The phosphorylation site of tau in the cerebrums and cerebellums of the NPC1+/+ and NPC1+/− mice at 24 and 40 weeks of age was also determined (Fig. 4, *b* and *c*, respectively). The phosphorylation state of tau and the total tau level in both samples demonstrated by AT-8 and T-46 did not differ between the NPC1+/+ and NPC1+/− mice (Fig. 4, *b* and *c*).

MAPK Was Activated in NPC1+/− Mouse Brains—Since our previous reports demonstrated that tau phosphorylation in NPC1-deficient cells is caused by enhanced MAPK activity (6, 17), the activity of tau kinases including MAPK was determined. Among the kinases examined, including MAPK/ERK1/2, GSK-3β, JNK, and Cdk5/p25, the levels of phospho-MAPK/ERK1/2 in the cerebrum and cerebellum of the NPC1+/− mice at 104–106 weeks of age increased compared with those for the NPC1+/+ mice (Fig. 5*a*), whereas the levels of phospho-GSK-3β, -JNK, and Cdk5/p25 remained unchanged (Fig. 5, *b*, *c*, and *d*). The activities of MAPK/ERK1/2 in the cerebrums and cerebellums of the NPC1+/+ and NPC1+/− mice at 24 and 40 weeks of age were also determined. The activities of MAPK/ERK1/2 in both samples did not differ between the NPC1+/+ and NPC1+/− mice (Fig. 5, *e* and *f*).

Cholesterol Level in Lipid Rafts Decreased in NPC1+/− Mouse Brains—Because the enhanced MAPK/ERK1/2 activity due to the decreased cholesterol level in the lipid rafts is suggested to induce tau phosphorylation in NPC1−/− mouse brains and NPC1−/− cells (6, 17), lipid compositions in the raft fractions isolated from the cerebral cortices of the NPC1+/+ and NPC1+/− mice were analyzed. The raft marker GM1 ganglioside was recovered in fractions 4 and 5, and another raft marker, flotillin-1, was recovered in fraction 5 (Fig. 6*c*). The cholesterol levels in fractions 4 and 5 isolated from the NPC1+/− brain were significantly lower than those in the same fractions isolated from the NPC1+/+ brain (Fig. 6*a*), whereas the levels of phospholipids in these fractions showed no significant difference between the two genotypes (Fig. 6*b*).

Level of ATP in NPC1+/+ and NPC1+/− Brains—Our previous study demonstrated that ATP levels in NPC1−/− organs including the brain, liver, and muscles as well as in NPC1−/− cultured neurons decrease compared with those in NPC1+/+ organs and neurons (22); thus, ATP level and ATP synthase activity in the aged NPC1+/+ and NPC1+/− brains were determined. As shown in Fig. 7, ATP levels in the cerebrum and cerebellum of the NPC1+/− mice at 104–106 weeks of age significantly decreased compared with those in the same brain areas of the NPC1+/+ mice (Fig. 7*a*). ATP synthase activity in the cerebellum of the aged NPC1+/− mice also decreased compared with that of the aged NPC1+/+ mice (Fig. 7*b*).

DISCUSSION

Here we demonstrate for the first time the unexpected phenomenon that neurodegeneration occurs in aged NPC1+/− mouse brains. This neuronal damage is accompanied by tau hyperphosphorylation and enhanced MAPK/ERK1/2 activity, which are observed in young NPC1−/− mouse brains and NPC1−/− cells (6, 17). The significant accumulation of cholesterol in neurons in the brain and the significant reduction in cholesterol level in raft fractions isolated from aged NPC1+/− cerebrums were also observed. These changes are found to depend on aging in NPC1+/− mice.

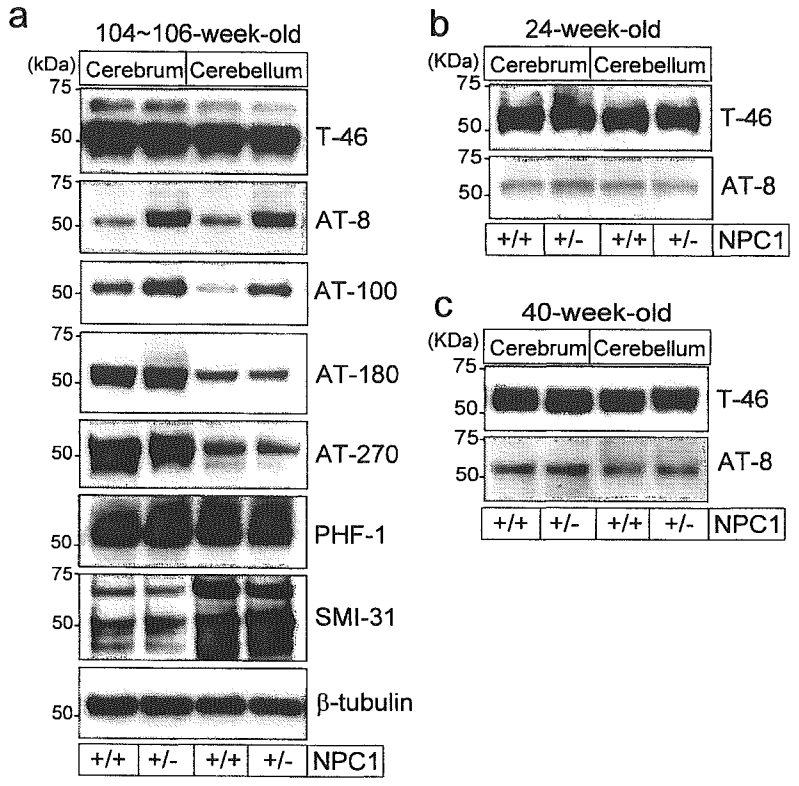

FIG. 4. **Immunoblot analysis of tau in cerebrum and cerebellum of 104–106-week-old NPC1+/+ and NPC1+/− mice.** *a*, equal amounts of postnuclear supernatant protein from the cerebrum and cerebellum were subjected to immunoblot analysis using the site-specific phospho-tau antibodies AT-8, AT-100, AT-180, AT-270, PHF-1, and SMI-31 in addition to an antibody that recognizes phospho-independent tau, T46, and the anti-β-tubulin antibody as an internal standard. Tau in the cerebrum and cerebellum of 24-week-old (*b*) and 40-week-old (*c*) NPC1+/+ and NPC1+/− mice was immunohistochemically analyzed using AT-8 and AT-100 antibodies.

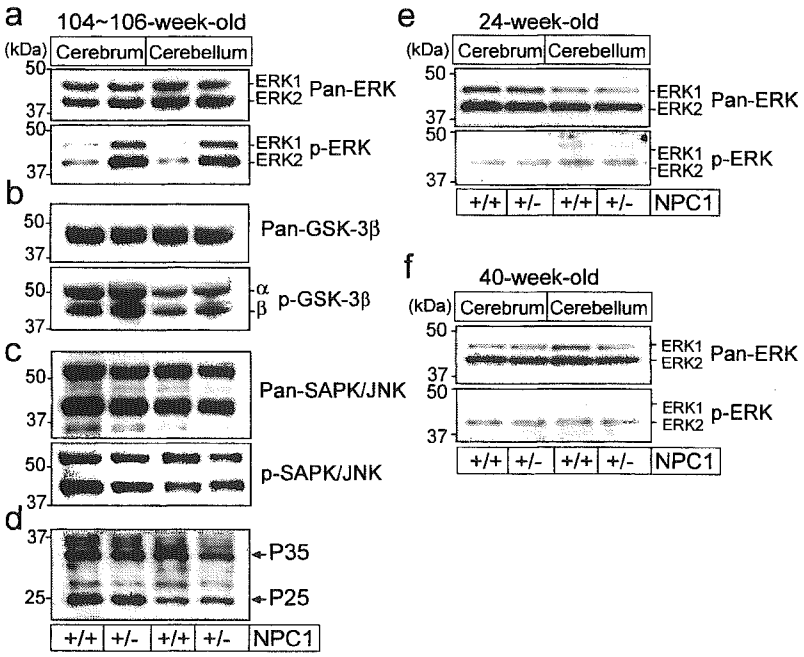

FIG. 5. **Immunoblot analysis of tau-directed kinases in cerebrum and cerebellum of 104–106-week-old NPC1+/+ and NPC1+/− mice.** Equal amounts of postnuclear supernatant protein from the cerebrum and cerebellum were subjected to immunoblot analysis using the monoclonal antibodies specific for pan-ERK1/2 and phospho-ERK (*p-ERK*) (*a*), pan-GSK-3β and phospho-GSK-3β (*p-GSK-3β*) (*b*), pan-SAPK/JNK and phospho-SAPK/JNK (*p-SAPK/JNK*) (*c*), and Cdk5 (*d*). Immunoblot analysis of ERK1/2 in the cerebrum and cerebellum of 24-week-old (*e*) and 40-week-old (*f*) NPC1+/+ and NPC1+/− mice was performed using anti-pan-ERK and anti-phospho-ERK antibodies.

NPC1 disease is a hereditary disorder that develops in an autosomal recessive manner; thus, it has been assumed that heterozygous carriers of NPC1 mutations do not develop any neurological symptoms during their entire life span (1). It has also been presumed that this is the case for NPC1+/− model mice. Therefore, little attention has been paid to whether NPC1+/− mice develop any symptoms with aging. To our surprise, however, the present study has clearly shown that neurodegeneration demonstrated as Purkinje cell loss accompanied by intracellular cholesterol accumulation and its deficiency in lipid rafts occurs in the aged NPC1+/− mouse brain. A few studies have investigated NPC1 heterozygotes and have shown that NPC1 heterozygotes have "intermediate" abnormalities in cholesterol metabolism at the nonneuronal cell level (23, 26, 27); however, it has been shown that there is no significant abnormality in terms of cholesterol metabolism in cultured NPC1+/− neurons (30) and young NPC1+/− brains (6). These lines of evidence suggest that cholesterol metabolism in the central nervous system changes and neurodegeneration accompanied by abnormal tau phosphorylation occurs only in aged NPC1+/− mice. The reason for the change in cholesterol metabolism found only in the aged NPC1+/− brains may be the expression of the NPC1 protein in NPC1+/− brains being approximately half that in NPC1+/+ brains (6), which may

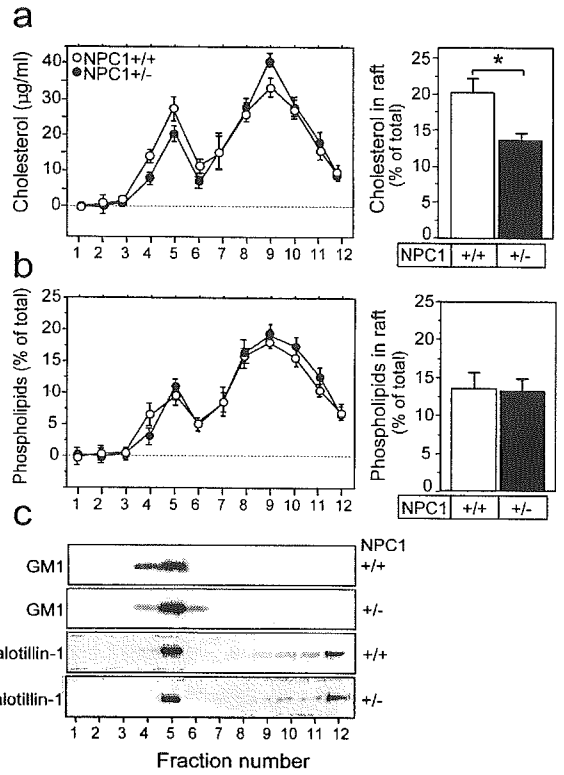

FIG. 6. **Distribution of cholesterol and phospholipids in raft fractions from brains of 104–106-week-old NPC1+/+ and NPC1+/− mice.** The cell homogenates of the cerebellar cortices of 104–106-week-old NPC1+/+ and NPC1+/− mice in the presence of 1% Triton X-100 were subjected to sucrose density gradient ultracentrifugation. The levels of cholesterol (*a*) and phospholipids (*b*) in each fraction were determined, and the distribution of such components across the fractions is shown. *c*, distribution of GM1 ganglioside and flotillin-1, markers for lipid rafts, across the fractions was determined as described under "Experimental Procedures." The levels of cholesterol (*a*, *right panel*) and phospholipids (*b*, *right panel*) in fractions 4 and 5 (raft fractions) are shown. Data represent the mean ± S.E. of six samples. Two independent experiments showed similar results. *, $p < 0.04$

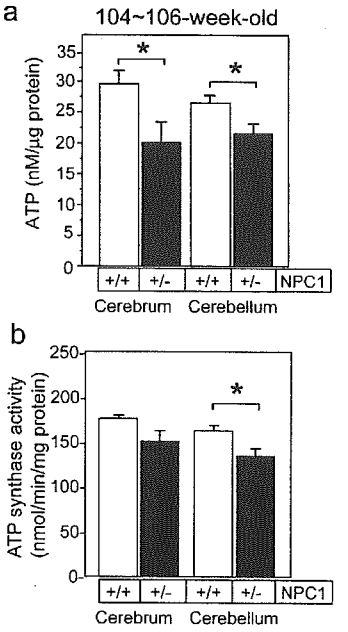

FIG. 7. **ATP level and ATP synthase activity in brains of 104–106-week-old NPC1+/+ and NPC1+/− mice.** *a*, ATP level was determined in the cerebrum and cerebellum isolated from the NPC1+/+ and NPC1+/− mice at 104–106 weeks of age. For each of the samples, equal amounts of protein were used to compare ATP level. Data show mean ± S.E. of five samples. Two independent experiments show similar results. *b*, the ATP synthase activities in mitochondria isolated from cerebrum and cerebellum of the NPC1+/+ and NPC1+/− mice at 104–106 weeks of age was determined. The fraction containing purified brain mitochondria was isolated as described previously (22). The enzymatic analysis was performed by measuring the rate of ATP synthesis from ADP (ATP synthesis). The results represent the mean ± S.E. of five different samples and are representative of two independent experiments. *, $p < 0.05$.

very slightly affect cellular cholesterol trafficking. As a result, it takes a longer time for neurons to show any abnormalities in terms of cholesterol accumulation in the late endosome/lysosome compartment and the subsequent shortage of cholesterol in other compartments.

Since a decreased cellular cholesterol level stimulates MAPK activity (17, 31) and tau phosphorylation (32), it is reasonable to postulate that a reduced cholesterol level in lipid rafts, due to impaired cholesterol trafficking, increases MAPK activity and enhances tau phosphorylation in aged NPC1+/− brains. This is the case for younger NPC1−/− brains; *i.e.* neurodegeneration in NPC1−/− brains is linked with an increased MAPK activity and enhanced tau phosphorylation induced by a sustained cholesterol shortage due to the absence of its trafficking (6, 17).

In addition, it is likely that impaired cholesterol trafficking and the resultant intracellular cholesterol accumulation may result in an increased cholesterol level in mitochondria, which induces mitochondrial dysfunction, thereby affecting ATP synthase activity and reducing cellular ATP level, because, as we have reported, both increased and decreased cholesterol level in the mitochondrial membrane cause mitochondrial dysfunction and reduce cellular ATP level, which causes neurodegeneration in the younger NPC1−/− mice (22). With these results taken together, it is possible that the altered cellular cholesterol metabolism enhances tau phosphorylation and decreases cellular ATP level, both of which synergistically or independently induce neuronal neurodegeneration. One may raise the questions of what causes neurodegeneration, enhanced tau phosphorylation or low ATP level, and whether these two pathways work independently or dependently. The present study cannot answer these questions. Previous studies demonstrated that mitochondrial dysfunction with energy depletion causes cell death (33, 34) and that tau abnormalities alone can cause neurodegenerative diseases (35, 36), indicating that each pathway can independently cause neuronal death. However, previous studies showed that there is a correlation between ATP level and the activity of tau kinases including MAPK/ERK1/2 (37, 38). These results enable us to assume that mitochondrial dysfunction with a decreased ATP level and the enhancement of tau phosphorylation synergistically contribute to neurodegeneration in aged NPC1+/− mouse brains.

Finally, the results of our present study, contrary to what has been assumed, suggest that heterozygous NPC1 mutations are a risk for neuronal impairment. Since the ratio of the population with heterozygous NPC1 mutations is estimated to be as high as 0.5% (1), our findings lead us to further examine whether heterozygous NPC1 mutations are a risk for tauopathy, including Alzheimer disease. These issues should be addressed in future studies.

REFERENCES

1. Patterson, M. C., Vanier, M. T., Suzuki, K., Morris, J. A., Carstea, E. D., Neufeld, E. B., Blanchette Mackie, E. J., and Pentchev, P. G. (2001) in *The Metabolic and Molecular Basis of Inherited Disease* (Scriver, C. R., Beaudet, A. L., Sly, W. S., and Valle, D., eds) pp. 3611–3633, McGraw-Hill Inc., New York
2. Liscum, L., Ruggiero, R. M., and Faust, J. R. (1989) *J. Cell Biol.* **108,** 1625–1636
3. Pentchev, P. G., Kruth, H. S., Comly, M. E., Butler, J. D., Vanier, M. T., Wenger, D. A., and Patel, S. (1986) *J. Biol. Chem.* **261,** 16775–16780

4. Kobayashi, T., Beuchat, M. H., Lindsay, M., Frias, S., Palmiter, R. D., Sakuraba, H., Parton, R. G., and Gruenberg, J. (1999) *Nat. Cell Biol.* **1,** 113–118
5. Cruz, J. C., and Chang, T. Y. (2000) *J. Biol. Chem.* **275,** 41309–41316
6. Sawamura, N., Gong, J. S., Garver, W. S., Heidenreich, R. A., Ninomiya, H., Ohno, K., Yanagisawa, K., and Michikawa, M. (2001) *J. Biol. Chem.* **276,** 10314–10319
7. Loftus, S. K., Morris, J. A., Carstea, E. D., Gu, J. Z., Cummings, C., Brown, A., Ellison, J., Ohno, K., Rosenfeld, M. A., Tagle, D. A., Pentchev, P. G., and Pavan, W. J. (1997) *Science* **277,** 232–235
8. Carstea, E. D., Morris, J. A., Coleman, K. G., Loftus, S. K., Zhang, D., Cummings, C., Gu, J., Rosenfeld, M. A., Pavan, W. J., Krizman, D. B., Nagle, J., Polymeropoulos, M. H., Sturley, S. L., Ioannou, Y. A., Higgins, M. E., Comly, M., Cooney, A., Brown, A., Kaneski, C. R., Blanchette-Mackie, E. J., Dwyer, N. K., Neufeld, E. B., Chang, T. Y., Liscum, L., Strauss, J. F., III, Ohno, K., Zeigler, M., Carmi, R., Sokol, J., Markie, D., O'Neill, R. R., van Diggelen, O. P., Elleder, M., Patterson, m. C., Brady, R. O., Vanier, M. T., Pentchev, P. G., and Tagle, D. A. (1997) *Science* **277,** 228–231
9. Liscum, L., and Klansek, J. J. (1998) *Curr. Opin. Lipidol.* **9,** 131–135
10. Neufeld, E. B., Wastney, M., Patel, S., Suresh, S., Cooney, A. M., Dwyer, N. K., Roff, C. F., Ohno, K., Morris, J. A., Carstea, E. D., Incardona, J. P., Strauss, J. F., III, Vanier, M. T., Patterson, M. C., Brady, R. O., Pentchev, P. G., and Blanchette-Mackie, E. J. (1999) *J. Biol. Chem.* **274,** 9627–9635
11. Garver, W. S., Heidenreich, R. A., Erickson, R. P., Thomas, M. A., and Wilson, J. M. (2000) *J. Lipid Res.* **41,** 673–687
12. Wojtanik, K. M., and Liscum, L. (2003) *J. Biol. Chem.* **278,** 14850–14856
13. Suzuki, K., Parker, C. C., Pentchev, P. G., Katz, D., Ghetti, B., D'Agostino, A. N., and Carstea, E. D. (1995) *Acta Neuropathol.* **89,** 227–238
14. Love, S., Bridges, L. R., and Case, C. P. (1995) *Brain* **118,** 119–129
15. Auer, I. A., Schmidt, M. L., Lee, V. M., Curry, B., Suzuki, K., Shin, R. W., Pentchev, P. G., Carstea, E. D., and Trojanowski, J. Q. (1995) *Acta Neuropathol.* **90,** 547–551
16. Bu, B., Li, J., Davies, P., and Vincent, I. (2002) *J. Neurosci.* **22,** 6515–6525
17. Sawamura, N., Gong, J. S., Chang, T. Y., Yanagisawa, K., and Michikawa, M. (2003) *J. Neurochem.* **84,** 1086–1096
18. Karten, B., Vance, D. E., Campenot, R. B., and Vance, J. E. (2003) *J. Biol. Chem.* **278,** 4168–4175
19. Walkley, S. U., Siegel, D. A., Dobrenis, K., and Zervas, M. (1998) *Ann. N. Y. Acad. Sci.* **845,** 188–199
20. Liu, Y., Wu, Y. P., Wada, R., Neufeld, E. B., Mullin, K. A., Howard, A. C., Pentchev, P. G., Vanier, M. T., Suzuki, K., and Proia, R. L. (2000) *Hum. Mol. Genet.* **9,** 1087–1092
21. Griffin, L. D., Gong, W., Verot, L., and Mellon, S. H. (2004) *Nat. Med.* **10,** 704–711
22. Yu, W., Gong, J. S., Ko, M., Garver, W. S., Yanagisawa, K., and Michikawa, M. (2005) *J. Biol. Chem.*
23. Kruth, H. S., Comly, M. E., Butler, J. D., Vanier, M. T., Fink, J. K., Wenger, D. A., Patel, S., and Pentchev, P. G. (1986) *J. Biol. Chem.* **261,** 16769–16774
24. Vanier, M. T., Wenger, D. A., Comly, M. E., Rousson, R., Brady, R. O., and Pentchev, P. G. (1988) *Clin. Genet.* **33,** 331–348
25. Vanier, M. T., Rodriguez-Lafrasse, C., Rousson, R., Gazzah, N., Juge, M. C., Pentchev, P. G., Revol, A., and Louisot, P. (1991) *Biochim. Biophys. Acta* **1096,** 328–337
26. Garver, W. S., Krishnan, K., Gallagos, J. R., Michikawa, M., Francis, G. A., and Heidenreich, R. A. (2002) *J. Lipid Res.* **43,** 579–589
27. Choi, H. Y., Karten, B., Chan, T., Vance, J. E., Greer, W. L., Heidenreich, R. A., Garver, W. S., and Francis, G. A. (2003) *J. Biol. Chem.* **278,** 32569–32577
28. Feng, B., Zhang, D., Kuriakose, G., Devlin, C. M., Kockx, M., and Tabas, I. (2003) *Proc. Natl. Acad. Sci. U. S. A.* **100,** 10423–10428
29. Michikawa, M., Fan, Q. W., Isobe, I., and Yanagisawa, K. (2000) *J. Neurochem.* **74,** 1008–1016
30. Henderson, L. P., Lin, L., Prasad, A., Paul, C. A., Chang, T. Y., and Maue, R. A. (2000) *J. Biol. Chem.* **275,** 20179–20187
31. Wang, P. Y., Liu, P., Weng, J., Sontag, E., and Anderson, R. G. (2003) *EMBO J.* **22,** 2658–2667
32. Fan, Q. W., Yu, W., Senda, T., Yanagisawa, K., and Michikawa, M. (2001) *J. Neurochem.* **76,** 391–400
33. Green, D. R., and Reed, J. C. (1998) *Science* **281,** 1309–1312
34. Lang-Rollin, I. C., Rideout, H. J., Noticewala, M., and Stefanis, L. (2003) *J. Neurosci.* **23,** 11015–11025
35. Hutton, M., Lendon, C. L., Rizzu, P., Baker, M., Froelich, S., Houlden, H., Pickering-Brown, S., Chakraverty, S., Isaacs, A., Grover, A., Hackett, J., Adamson, J., Lincoln, S., Dickson, D., Davies, P., Petersen, R. C., Stevens, M., de Graaff, E., Wauters, E., van Baren, J., Hillebrand, M., Joosse, M., Kwon, J. M., Nowotny, P., Che, L. K., Norton, J., Morris, J. C., Reed, L. A., Trojanowski, J., Basun, H., Lannfelt, L., Neystat, M., Fahn, S., Dark, F., Tannenberg, T., Dodd, P. R., Hayward, N., Kwok, J. B., Schofield, P. R., Andreadis, A., Snowden, J., Craufurd, D., Neary, D., Owen, F., Oostra, B. A., Hardy, J., Goate, A., van Swieten, J., Mann, D., Lynch, T., and Heutink, P. (1998) *Nature* **393,** 702–705
36. Poorkaj, P., Bird, T. D., Wijsman, E., Nemens, E., Garruto, R. M., Anderson, L., Andreadis, A., Wiederholt, W. C., Raskind, M., and Schellenberg, G. D. (1998) *Ann. Neurol.* **43,** 815–825
37. Bush, M. L., Miyashiro, J. S., and Ingram, V. M. (1995) *Proc. Natl. Acad. Sci. U. S. A.* **92,** 1861–1865
38. Mizukami, Y., Iwamatsu, A., Aki, T., Kimura, M., Nakamura, K., Nao, T., Okusa, T., Matsuzaki, M., Yoshida, K., and Kobayashi, S. (2004) *J. Biol. Chem.* **279,** 50120–50131

Available online at www.sciencedirect.com
SCIENCE DIRECT
Brain Research 1043 (2005) 218–224
BRAIN RESEARCH
www.elsevier.com/locate/brainres

Short communication

Substance P immunoreactive cell reductions in cerebral cortex of Niemann–Pick disease type C mouse

Myeung Ju Kim[a], Jaewoo Kim[b], Brian Hutchinson[b], Makoto Michikawa[c], Choong Ik Cha[d], Bonghee Lee[b,e,*]

[a]*Department of Anatomy, Dankook University College of Medicine, Anseo-dong, Cheonan-si, Chungnam, South Korea*
[b]*Department of Anatomy, Cheju National University College of Medicine, 1 Ara 1 Dong, Jeju, Jeju-do 690-756, South Korea*
[c]*Section of Pathophysiology and Neurobiology, Department of Alzheimer's Disease Research, National Institute for Longevity Sciences, 36-3 Gengo, Morioka, Obu, Aichi 474-8522, Japan*
[d]*Department of Anatomy, Seoul National University College of Medicine, 28 Yongon-Dong, Chongno-Gu, Seoul 110-799, South Korea*
[e]*Institute of Medical Science, Cheju National University College of Medicine, Ara 1 Dong, Jeju, Jeju-do 690-756, South Korea*

Accepted 4 February 2005
Available online 1 April 2005

Abstract

Niemann–Pick disease type C (NPC) is characterized by progressive neurodegeneration and arises from mutations in the NPC1 gene. Cholesterol has received most attention in the pathogenesis of NPC, but normalizing lipid levels in humans or mouse does not prevent neurodegeneration. In NPC mouse, neuronal degeneration in the cerebellum is the most commonly detected change, and thus previous studies have tended to focus on the cerebellum, especially Purkinje cells. Although numerous peptides have been found in the mammalian central nervous system, little data on neurotransmitters in NPC are available, and information on neurotransmitter system abnormalities could explain the complex and characteristic deficits of NPC. Thus, we performed an immunohistochemical study on NPC mouse cortices to compare cell numbers exhibiting vasoactive intestinal polypeptide (VIP), neuropeptide Y (NPY), and substance P (SP) immunoreactivity. In terms of VIP and NPY-immunoreactive (ir) cell numbers in the cerebral cortex, SP-ir cells were significantly reduced by about 90% in NPC $^{(-/-)}$ versus NPC $^{(+/+)}$ mouse, and were also mildly decreased in frontal and parietal NPC $^{(+/-)}$ versus NPC $^{(+/+)}$ mouse cortex. This study demonstrates for the first time, reduced number of SP-ir cells in the NPC mouse cortex.

Theme: Disorders of the nervous system
Topic: Degenerative disease: other

Keywords: Niemann–Pick disease type C (NPC); Mouse cortex; Vasoactive intestinal polypeptide (VIP); Neuropeptide Y (NPY); Substance P (SP); Immunohistochemistry

Niemann–Pick disease type C (NPC) arises from mutations in the NPC1 gene on chromosome 18 [3], and is a fatal autosomal recessive neurovisceral disorder [21] characterized by the progressive neurodegeneration of the central nervous system (CNS) [6], which leads to premature death [23]. Cells lacking functional NPC1 accumulate cholesterol in the lysosomal and late endosomal compartments [12]. Cellular lesions in NPC patients are characterized by impaired LDL (low-density lipoprotein)-derived cholesterol transport from lysosomes, which results in lysosomal cholesterol sequestration [28]. In addition to cholesterol, neutral glycolipids and monosialogangliosides accumulate in the brains of NPC patients [23]. These lipid disturbances are essentially localized to gray matter. NPC patients exhibit increasing loss of motor control, seizures, and other neuropathological symptoms [22]. Like other lysosomal storage diseases, NPC disease is associated with

* Corresponding author. Department of Anatomy, Cheju National University College of Medicine, 1 Ara 1 Dong, Jeju, Jeju-do 690-756, South Korea. Fax: +82 64 702 2687.
E-mail address: bhlee1@cheju.ac.kr (B. Lee).

0006-8993/$ - see front matter © 2005 Elsevier B.V. All rights reserved.
doi:10.1016/j.brainres.2005.02.052

axonal abnormalities (spheroids, meganeurites, and axonal dystrophy) and demyelination of the corpus callosum [8]. A similar metabolic disorder has been previously described in Balb/C [27] and C57Bl/KsJ mouse [1]. Every organ manifests an accumulation of unesterified cholesterol and thus the whole body pool of sterol increases almost 3-fold by the time these animals are 11 weeks old [8]. Many neurons in the central nervous system show similar cholesterol-rich inclusions, as evidenced by positive fluorescence in filipin-stained brain sections [14]. However, normalizing lipid levels in humans and mouse does not prevent neurodegeneration [23]. Furthermore, evidence indicates that the concentrations of cholesterol and of its cytotoxic oxygenated derivatives are not increased in the brain of NPC mouse [24]. Therefore, a single mechanism associated with lipid or cholesterol is unlikely to account for NPC pathology.

Numerous peptides are found in the mammalian central nervous system. Neuropeptides found in high concentrations in the cerebral cortex include vasoactive intestinal polypeptide (VIP), neuropeptide Y (NPY), and substance P (SP) [4]. Thus, details of abnormalities of neurotransmitter and of their receptors could explain the complex and characteristic deficits of NPC [5], and comparisons between NPC neurotransmitter systems at disease onset and in the non-pathogenic state could be highly informative. However, previous studies on neurotransmitter expression in NPC mouse have focused primarily on the cerebellum, and especially on Purkinje cells, since neuronal degeneration in the cerebellum and associated brain stem structures is the most commonly detected change in NPC mouse, and is consistent with the development of tremor and ataxia [24]. However, a few have attempted to characterize the cell contents of regions like the cerebral cortex. Yadid et al. [28] found increased gamma amino butyric acid (GABA) and reduced serotonin levels in the NPC mouse cortex. These may be linked to the altered mouse exploratory behavior because GABA and serotonin are major regulators of emotional behavior like fear and anxiety [28]. Thus, we conjectured that changes in neurotransmitters or neuropeptides distributions in the cortex of NPC model mouse might provide information concerning NPC. We were particularly interested in the changes of immunoreactive (ir) cell number, which were stained by various neurotransmitters such as VIP, NPY, and SP. In this study, we quantitatively determined the cell numbers showing the VIP, NPY, and SP immunoreactivity (IR) using immunohistochemistry in the homogenously NPC 1 mutated mouse (−/−) cortex and compared these with those of the heterogenous (+/−) and wild (+/+) types.

BALB/c mice carrying the mutated NPC 1 gene were originally obtained from Dr. Michikawa (Dementia Research, NILS, Aichi, Japan) [15]. The mouse used in this study was 11 weeks old. For each VIP, NPY, and SP antibody, six NPC $^{(+/+)}$, five NPC $^{(+/-)}$, and five NPC $^{(-/-)}$ animals of both sexes were used. Additionally, we used all three types of mouse [six NPC $^{(+/+)}$, five NPC $^{(+/-)}$, and five NPC $^{(-/-)}$] at 4 weeks of age to compare developmental SP-ir cell number changes. Animals were treated in accordance with the *NIH Guide for the Care and Use of Laboratory Animals* (NIH publication No. 80-23, revised in 1996). Animals were anesthetized with pentobarbital (100 mg/kg, i.p.) and perfused transcardially with ice-cold 4% paraformaldehyde in 0.02 M phosphate-buffered saline (PBS, pH 7.4). Brains were cryoprotected in a series of cold sucrose solutions, and sectioned coronally at 30 μm on a cryostat. Immunohistochemistry was performed using the previously described free-floating method [4]. Rabbit anti-rat VIP (Diasorin, Cat No. 20077), NPY (Diasorin, Cat. No. 22940), and SP (Diasorin, Cat. No. 20064) antibodies were used as main primary antibodies at a final concentration of 1.5 mg/ml. In addition, we used another SP primary antibody (Chemicon, Cat No. MAB 356 at a dilution ratio of 1:3000) to certify the reliability of our immunohistochemical staining results. Some of the sections were reacted without primary antiserum, whereas others were exposed to a primary antiserum (0.06 mg/ml) that had been preabsorbed for 24 h with cognate peptide (0.1 mg/ml). No NPC $^{(+/+)}$ mouse brain sections showed any of the IR described in this report (Figs. 1B, C). All three types of mouse brain sections were stained together, thus eliminating experimental condition differences. To determine whether cell loss had occurred in NPC $^{(-/-)}$ mouse, we performed cresyl-violet staining in the mouse cortex. However, in 11-week-old NPC $^{(-/-)}$ mouse, we did not find any significant decrease in cell numbers in all the cortices of NPC $^{(-/-)}$ versus NPC $^{(+/+)}$ or NPC $^{(+/-)}$ by cresyl-violet staining (Figs. 1C–E). For the comparative analysis of neurotransmitters (VIP, NPY, SP), we selected 5 slides of each cortical area from each mouse, and counted all specifically stained cells in corresponding areas (Tables 1, 2) of mouse cerebral cortex for each primary antibody by optical microscopy. The Student's *t* test was used to determine whether changes in ir cell numbers in each cortical area were statistically significant (Table 2).

Prominent VIP-ir cells were observed throughout the cortices of three mouse types [NPC $^{(+/+)}$, NPC $^{(+/-)}$, NPC $^{(-/-)}$]. These were mainly present in layers II and III (Figs. 2A–C) although they were distributed in all layers of the cerebral cortex. VIP-ir cells were predominantly bipolar, i.e., with ovoid somata and dendrites oriented perpendicular to the pial surface (Figs. 2A–C). This distribution pattern was well preserved and no significant differences were observed between the cortices of the three mouse types (Figs. 2A–C, Table 1). NPY-IR showed a preferential distribution in cells of the II/III and V/VI layers. Cortical cells exhibited NPY-IR in the dendritic trees of bipolar and multipolar arrangements, and their cell bodies were fully stained in all three mouse types (Figs. 2G–I). When we compared all three mouse types, we were unable to find notable differences in the number of NPY-ir cells across mouse cortical areas (Table 2). A slight decrease of NPY-ir cell number was observed in the retrosplenial granular/

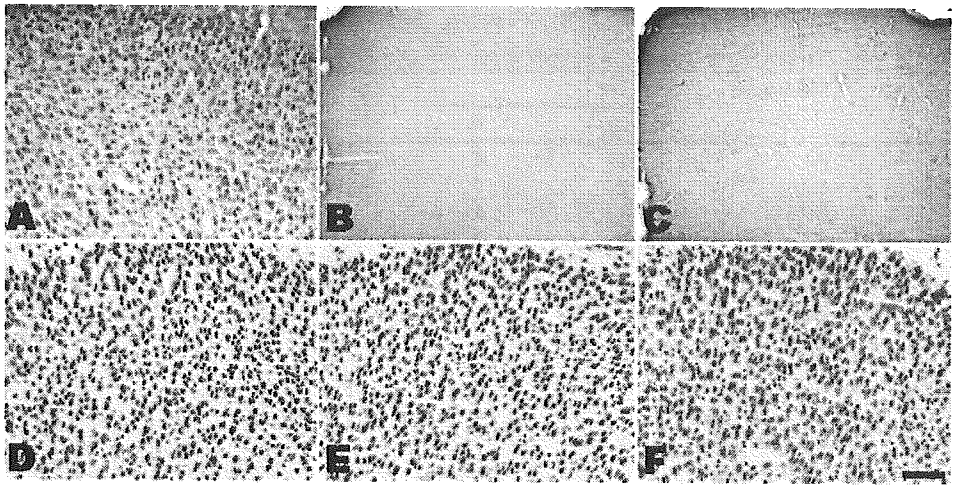

Fig. 1. In the frontal cortex area 1 of 11-week-old NPC $^{(+/+)}$ mouse, the SP (Chemicon, Cat No. MAB 356) immunoreactivities (IR) were largely confined to cell bodies and their proximal dendrites of IV–VI layers (A). By cresyl-violet staining, there were no cell number differences in the 11-week-old NPC $^{(-/-)}$ mouse (F) versus age-matched NPC $^{(+/+)}$ (D) or NPC $^{(+/-)}$ (E) mouse cortex. Sections that were reacted with primary SP antiserum [Cat. No. 20064 (B), and MAB 356 (C)] that had been preincubated for 24 h with cognate peptide did not exhibit any IR. Scale bars = 100 μm in A, D, E, F, 200 μm in B, C.

agranular NPC $^{(-/-)}$ compared with NPC $^{(+/+)}$ cortex (Table 1), where some individual variations in the NPY-ir cell number were present. In the 11-week-old NPC $^{(+/+)}$ mouse cortex, many SP-ir cell bodies were observed in the frontal, parietal, temporal, and occipital cortex. SP-ir cell bodies were observed in layers II–VI, and the majority of cells in NPC $^{(+/+)}$ mouse were bipolar or multipolar in shape (Fig. 2D). In the deeper layers of the 11-week-old NPC $^{(+/+)}$ mouse cortex, particularly layers V and VI, many arrays of SP-containing fibers were observed (Fig. 2D). These fibers were oriented perpendicular to the pial surface, and appeared to be fibers of passage with few varicosities (Figs. 2D, 3J). SP-ir cells in 11-week-old NPC $^{(+/-)}$ mouse (Figs. 2E, 3B, E, H) were similar in pattern to those in NPC $^{(+/+)}$ mouse (Figs. 2D, 3A, D, G) and were observed across all cortical areas. The number of SP-ir cells was severely decreased (>70%) in all areas of the 11-week-old NPC $^{(-/-)}$ mouse cortex (Figs. 2F, 3C, F, I, K) versus those of NPC $^{(+/+)}$ mouse (Figs. 2D, 3A, D, G, J, Tables 1, 2). When compared with 11-week-old NPC $^{(+/+)}$ mouse, changes in 11-week-old NPC $^{(+/-)}$ were variable in each cortical area. Moderate (50–70%) SP-ir cell reductions were observed in the frontal cortex 1 (Fig. 2E, Tables 1, 2), 2, and 3 and parietal cortex 1 (Figs. 3A–C, Tables 1, 2). Mild (15–50%) SP-ir cell reductions were observed in the parietal

Table 1
The number of VIP, NPY, and SP-ir neurons in each area of NPC $^{(+/+)}$, NPC $^{(+/-)}$, and NPC $^{(-/-)}$ mice cerebral cortex

		VIP			NPY			SP		
		(+/+)	(+/−)	(−/−)	(+/+)	(+/−)	(−/−)	(+/+)	(+/−)	(−/−)
Frontal	Fr1	78.1 ± 5.7	77.5 ± 4.3	76 ± 5.5	35.5 ± 5.7	35.7 ± 6.2	36.1 ± 4.9	673.2 ± 56.9	315.9 ± 36.9	34.2 ± 5.3
	Fr2	35.1 ± 8.9	35.2 ± 9.3	34.9 ± 10.2	23.8 ± 2.4	24.6 ± 8.1	23.3 ± 1.4	302.6 ± 37.3	143.1 ± 32.0	25.6 ± 2.6
	Fr3	51.6 ± 5.2	49.9 ± 9.8	52.1 ± 9.7	37.8 ± 8.4	38.1 ± 2.1	36.9 ± 10.6	441.3 ± 18.7	202.8 ± 10.6	13.3 ± 1.9
Cingulate		53.2 ± 6.4	53.8 ± 7.7	52.5 ± 7.4	32.6 ± 1.0	32.1 ± 6.3	30.4 ± 4.3	438.4 ± 24.9	415.5 ± 22.8	12.9 ± 2.6
Parietal	Par1	79.3 ± 2.4	80.1 ± 5.3	79.4 ± 8.6	21.7 ± 6.8	20.8 ± 1.4	21.9 ± 7.1	620.1 ± 53.4	390.8 ± 31.5	68.3 ± 7.4
	Par2	67.5 ± 5.1	68.3 ± 9.2	66 ± 6.9	19.1 ± 5.2	18.8 ± 2.7	18.6 ± 6.7	525.8 ± 64.8	432.5 ± 27.3	56.5 ± 2.8
Temporal	Te1	72.8 ± 3.5	71.6 ± 10.8	72.3 ± 7.2	23.7 ± 8.3	22.5 ± 9.4	23.1 ± 1.5	403.4 ± 46.1	389 ± 21.3	92.7 ± 7.1
	Te2	77.4 ± 5.5	77.1 ± 4.6	76.9 ± 8.3	18.0 ± 4.8	19.5 ± 4.2	17.6 ± 2.4	433.2 ± 29.8	428.6 ± 33.2	97.9 ± 10.7
	Te3	52.8 ± 8.2	52.6 ± 5.4	53 ± 5.7	17.1 ± 8.2	18.8 ± 2.1	17.3 ± 7.4	295.5 ± 18.7	292.4 ± 16.2	67.4 ± 9.3
Occipital	Oc2M	73.8 ± 6.2	73.6 ± 10.4	74 ± 8.7	33.8 ± 8.9	36.8 ± 7.9	36.5 ± 5.9	632.8 ± 21.7	598.1 ± 23.9	43.9 ± 5.2
	Oc2L	56.2 ± 6.2	55.8 ± 5.5	56.1 ± 9.5	23.6 ± 3.6	24.8 ± 3.5	24.3 ± 6.2	481.3 ± 42.3	468.5 ± 35.6	32.6 ± 2.4
	Oc1M	49.5 ± 9	48.9 ± 5	48.5 ± 8.2	25.3 ± 6.4	24.7 ± 2.8	25.1 ± 4.3	423.9 ± 29.6	409.6 ± 32.5	28.2 ± 1.3
	Oc1B	81.2 ± 6.2	80.2 ± 4.3	80.6 ± 5.4	28.8 ± 8.7	27.9 ± 1.8	28.2 ± 3.2	685.4 ± 63.1	653.4 ± 70.8	46.8 ± 3.4
Perirhinal area		76.1 ± 8.2	76.8 ± 9.1	76.5 ± 8.3	17.9 ± 9.1	17.5 ± 7.4	16.9 ± 8.4	68.2 ± 15.7	59.2 ± 13.6	8.8 ± 2.2
Retrosplenial granular and agranular cortex		52 ± 4.8	51.7 ± 8.6	51.8 ± 8.9	21.7 ± 2.2	17.6 ± 4.5	18.5 ± 3.9	467.8 ± 38.4	413.5 ± 52.3	13.4 ± 1.7
Piriform cortex		67.5 ± 11.3	66.8 ± 8.3	67 ± 9.6	13.0 ± 3.8	12.4 ± 2.9	13.1 ± 4.5	187.0 ± 25.3	172.2 ± 21.9	10.3 ± 2.5

Data = means ± SE. (+/+) = NPC $^{(+/+)}$; (+/−) = NPC $^{(+/-)}$; (−/−) = NPC $^{(-/-)}$.

Table 2
Changes of the numbers of VIP, NPY, and SP-immunoreactive neurons in each area of the NPC $^{(+/-)}$, NPC $^{(-/-)}$[a]

Area	Subdivision	VIP		NPY		SP	
		(+/−)	(−/−)	(+/−)	(−/−)	(+/−)	(−/−)
Frontal	Fr1	0	0	0	0	− −[b]	− − −[b]
	Fr2	0	0	0	0	− −[b]	− − −[b]
	Fr3	0	0	0	0	− −[b]	− − −[b]
Cingulate		0	0	0	0	0	− − −[b]
Parietal	Par1	0	0	0	0	− −[b]	− − −[b]
	Par2	0	0	0	0	−[b]	− − −[b]
Temporal	Te1	0	0	0	0	0	− − −[b]
	Te2	0	0	0	0	0	− − −[b]
	Te3	0	0	0	0	0	− − −[b]
Occipital	Oc2M	0	0	0	0	0	− − −[b]
	Oc2L	0	0	0	0	0	− − −[b]
	Oc1M	0	0	0	0	0	− − −[b]
	Oc1B	0	0	0	0	0	− − −[b]
Perirhinal area		0	0	0	0	0	− − −[b]
Retrosplenial granular and agranular cortex		0	0	−	0	0	− − −[b]
Piriform cortex		0	0	0	0	0	− − −[b]

[a] The data were classified into 4 categories comparing the immunoreactive (ir) cell number in NPC (+/−), NPC (−/−) with ir cell number of NPC (+/+) according to the % of counted cell number [0, no change (−15–15%); −, mild decrease (15–50%);− −, moderate decrease (50–75%);− − −, severe decrease (>75%)] and counted the number of cells graded '0, −, − −, − − −'.
[b] Statistically significant area ($P < 0.05$).

cortex 2 (Tables 1, 2). In particular, few cells showed SP-IR in the occipital cortex (Fig. 3I). At the cellular level, SP-IR in the 11-week-old NPC $^{(+/+)}$ mouse cortex was mainly localized in cell bodies and cytoplasmic processes (Fig. 3J). However, dendrites of SP-ir cells in the cortex of 11-week-old NPC $^{(-/-)}$ mouse were markedly shorter and barely observed (Fig. 3K). Morphologically, the dendrites of SP-ir cells branched several times in 11-week-old NPC $^{(+/+)}$ mouse

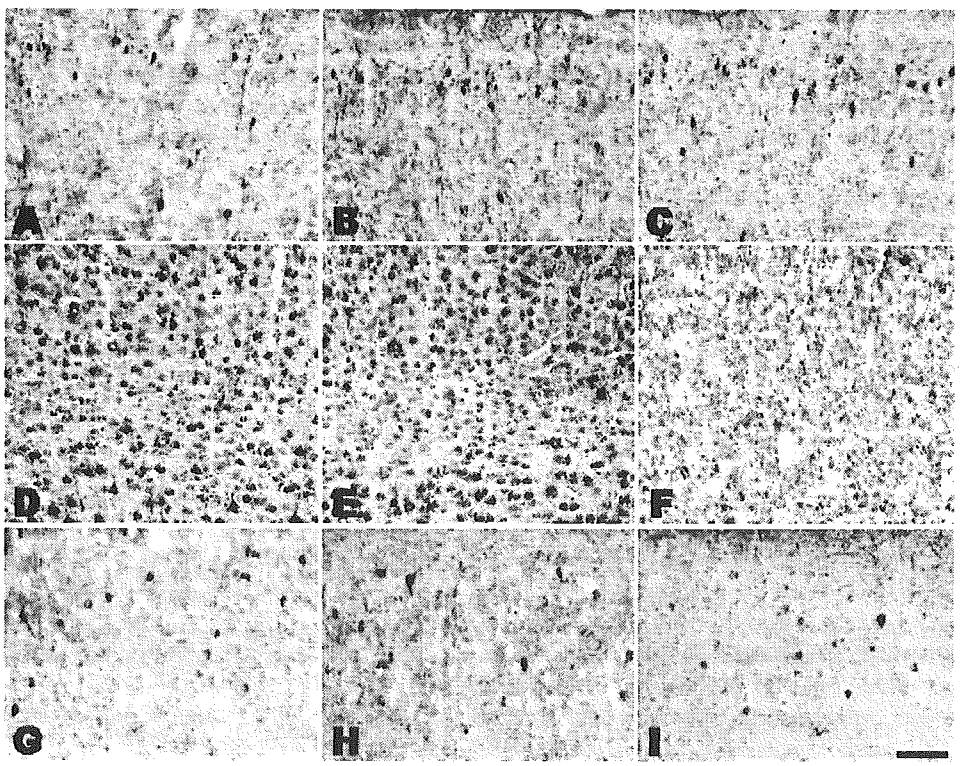

Fig. 2. Changes in the number of VIP (A, B, C), SP (D, E, F), and NPY (G, H, I) immunoreactive (ir) cells in the frontal cortex area 1 of NPC $^{(-/-)}$ (C, F, I), NPC $^{(+/-)}$ (B, E, H), and NPC $^{(+/+)}$ (A, D, G). A significant reduction of SP-ir cell number and the small number of shortened dendritic branches were observed in frontal cortex area 1 of the NPC $^{(-/-)}$ (F). VIP and NPY-ir cells in the frontal cortex area 1 show no significant differences among the three mice models. Scale bar = 100 μm.

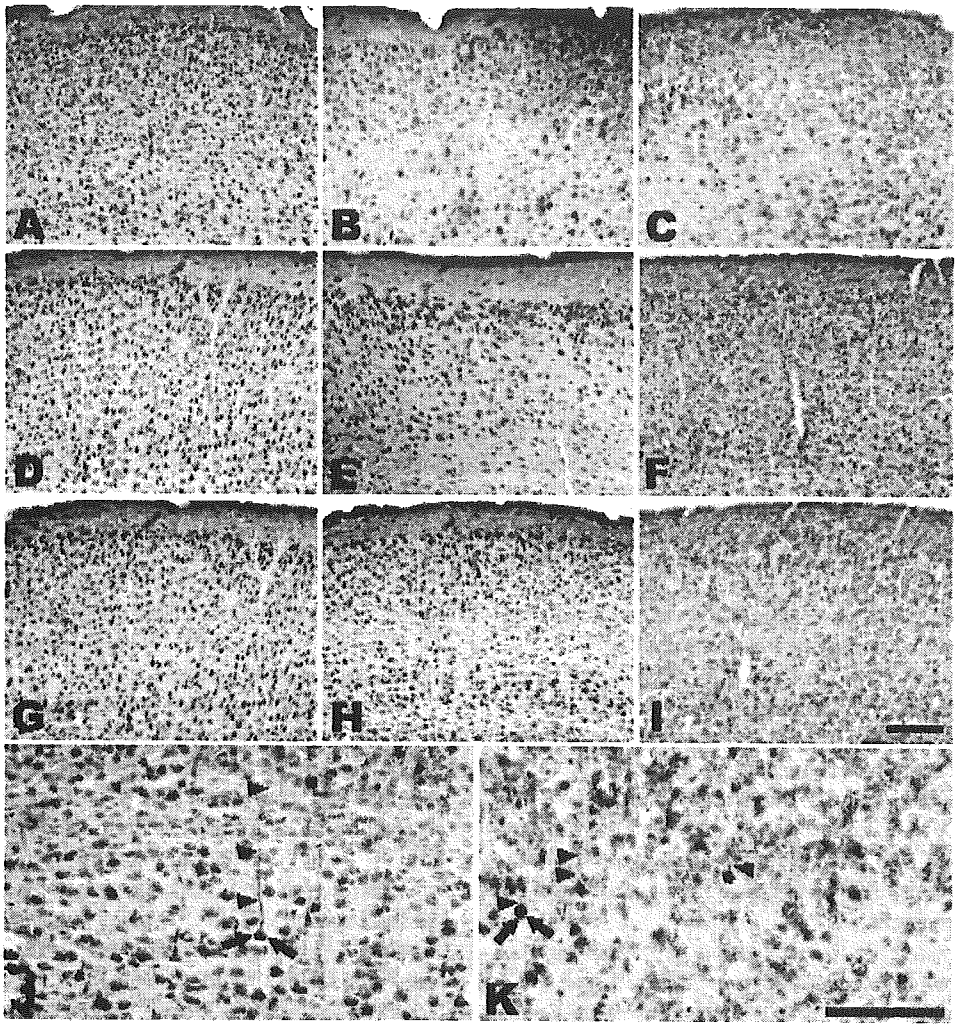

Fig. 3. Changes in the numbers of SP immunoreactive (ir) cells in the cerebral cortex of 11-week-old NPC $^{(-/-)}$ (C, F, I), NPC $^{(+/-)}$ (B, E, H), and NPC $^{(+/+)}$ (A, D, G) mouse. Both in NPC $^{(+/+)}$ and in NPC $^{(+/-)}$ mouse, SP-ir cells were present in II–VI layers of parietal cortex 1 (A, B), and the temporal cortex area 1 (D, E) and occipital cortex area 1 (G, H). SP immunoreactivity was largely localized in cell bodies and proximal dendritic processes. In NPC $^{(-/-)}$ mouse, the number of SP-ir neurons was markedly reduced and their dendritic branches were hardly observed, especially in occipital area 1 (I). Magnified images of SP-ir neurons in frontal cortex 1 of NPC $^{(+/+)}$ (J), and NPC $^{(-/-)}$ mouse (K) showing that SP-ir neurons in NPC $^{(+/+)}$ (J) have long and prominent processes compared to those of NPC $^{(-/-)}$ mouse (K). The arrows (J, K) indicate the overall sizes of SP-ir somata. SP-ir somata of NPC $^{(-/-)}$ mouse were larger than those of NPC $^{(+/+)}$ mouse. The arrowheads (J, K) denote dendrite lengths of large neurons. Scale bar = 100 μm in A–I, 100 μm in J, K.

(Fig. 3J). Interestingly, some SP-ir cells in the 11-week-old NPC $^{(-/-)}$ mouse cortex were larger than those in NPC $^{(+/+)}$ mouse though the number of SP-ir cells were reduced (Fig. 3K). Distinct localization of SP-ir cells was also observed throughout the cortices of three mice types [NPC $^{(+/+)}$, NPC $^{(+/-)}$, NPC $^{(-/-)}$] at 4 weeks of age (Fig. 4). In layer V/VI, the majority of cells in 4-week-old NPC $^{(+/+)}$ mouse cortex (i.e., frontal, occipital cortex) were bipolar or multipolar in shape (Fig. 4). When we compared all three mouse types, there were no statistically significant differences in the number of SP-ir cells across mouse cortical areas (Figs. 1D–F). The IR of cell bodies was dense in all population of stained cells. The dendritic staining using SP antibody was relatively confined to proximal portions of the dendritic tree (Fig. 4). Further, in the layer V of occipital cortex area 1, many arrays of SP-containing fibers were observed (Fig. 4D).

The present study provides first morphological evidences of VIP, NPY, and SP-ir cell number in the NPC $^{(-/-)}$ mouse cortex as well as NPC $^{(+/+)}$ and NPC $^{(+/-)}$, and provides information on the altered distribution patterns of those neuropeptides. In the NPC $^{(-/-)}$ versus NPC $^{(+/+)}$ or NPC $^{(+/-)}$ mouse cortex, VIP and NPY-ir cells were not decreased, but SP-ir cells in frontal cortex areas 1, 2, and 3, occipital cortex areas 1 and 2, and retrosplenial granular/agranular and piriform cortices showed >90% reductions. Spatial selective changes in neuropeptide systems have also been reported in neurodegenerative diseases such as Alzheimer's disease (AD). With regard to VIP, 20–30% decreases in VIP-ir were reported in the temporal lobes of AD patients [17], and another study also found reduced levels of this peptide in the insular and angulate cortices of AD patients [2]. However, other investigators found no change in VIP [20] and NPY [7]